Open access • Journal Article • DOI:10.1089/ARS.2018.7690

# Structural and functional characterization of the globin-coupled sensors of Azotobacter vinelandii and Bordetella pertussis 

Francesca Germani, Marco Nardini, Amy De Schutter, Bert Cuypers ...+9 more authors

**Institutions:** University of Antwerp, University of Milan, University of Parma, University of Genoa

**Published on:** 14 Jan 2020 - Antioxidants & Redox Signaling (Mary Ann Liebert Inc.)

**Topics:** Azotobacter vinelandii, Bordetella pertussis and Globin

Structural and functional characterization of the globin-coupled sensors of *Azotobacter vinelandii* and *Bordetella pertussis*

Antioxidants and Redox Signaling

DOI: 10.1089/ars.2018.7690


Forum Original Research Communication

# Structural and functional characterization of the globin-coupled sensors of *Azotobacter vinelandii* and *Bordetella pertussis*

Francesca Germani[1], Marco Nardini[2], Amy De Schutter[3], Bert Cuypers[3], Herald Berghmans[1], Marie-Louise Van Hauwaert[1], Stefano Bruno[4], Andrea Mozzarelli[4], Luc Moens[1], Sabine Van Doorslaer[3], Martino Bolognesi[2], Alessandra Pesce[5,*], and Sylvia Dewilde[1,*]

[1] Department of Biomedical Sciences, University of Antwerp, Universiteitsplein 1, B-2610 Wilrijk, Belgium

[2] Department of Biosciences, University of Milano, Via Celoria 26, I-20133 Milan, Italy

[3] Department of Physics, University of Antwerp, Universiteitsplein 1, B-2610 Wilrijk, Belgium

[4] Department of Pharmacy, University of Parma, Parco Area delle Scienze 23/A, 43124 Parma, Italy

[5] Department of Physics, University of Genova, Via Dodecaneso 33, I-16146 Genova, Italy

[*]Authors to whom correspondence should be addressed; *e-mail*: sylvia.dewilde@uantwerpen.be, *tel*: +32-03-265-2323; *e-mail*: pesce@fisica.unige.it, *tel*: +39-010-353-6243

**Running title:** Structure and function of globin-coupled sensors.

**Keywords:** heme-based sensor, oxygen affinity, c-di-GMP and enzyme specificity, biofilm, crystal structure.

word count (excluding references and figure legends): 8288

reference numbers: 75

number of greyscale illustrations: 1 Figure and 4 Tables

number of color illustrations: 6 Figures

Antioxidants and Redox Signaling
Structural and functional characterization of the globin-coupled sensors of *Azotobacter vinelandii* and *Bordetella pertussis* (DOI: 10.1089/ars.2018.7690)
This paper has been peer-reviewed and accepted for publication, but has yet to undergo copyediting and proof correction. The final published version may differ from this proof.

**Abstract**

***Aims:*** Structural and functional characterization of the globin coupled sensors (GCS) of *Azotobacter vinelandii* (*Av*GReg) and *Bordetella pertussis* (*Bpe*GReg).

***Results:*** UV/Vis and RR spectroscopies confirm the presence in *Av*GReg and *Bpe*GReg of a globin domain capable of reversible gaseous ligand binding. In *Av*GReg an influence of the transmitter domain on the heme proximal region of the globin domain can be seen, and $k'_{CO}$ is higher than for other GCSs. The $O_2$ binding kinetics suggest the presence of an open and a closed conformation. As for *Bpe*GReg, the fully oxygenated *Av*GReg show a very high DGC activity. The CO rebinding to *Bpe*GReg indicates that intra- and intermolecular interactions influence the ligand binding. The globin domains of both proteins (*Av*GReg-Gb and *Bpe*GReg-Gb*) share the same GCS fold, a similar proximal but a different distal side structure. They homodimerize through a G-H helical bundle as in other GCS. However, *Bpe*GReg-Gb* shows also a second dimerization mode.

***Innovation*****:** This paper extends our knowledge on the GCS proteins and contributes to a better understanding of the GCSs' role in the formation of bacterial biofilms.

***Conclusions:*** *Av*GReg and *Bpe*GReg conform to the GCS family, share a similar overall structure but they have different properties in terms of the ligand binding. In particular, *Av*GReg shows an open and closed conformation that in the latter form will very tightly bind oxygen. *Bpe*GReg has only one closed conformation. In both proteins, it is the fully oxygenated GCS form that catalyzes the production of the second messenger.

## Introduction

Globin coupled sensors (GCSs) are heme-based molecules widespread in Bacteria and Archaea, consisting of chimeric proteins characterized by an N-terminal globin sensor domain coupled to a variety of C-terminal transmitter domains. Classification based on the function of the latter distinguishes: diguanylate cyclase (DGC), phosphodiesterase (PDE), histidine kinase, methyl-accepting chemotaxis and a transmembrane function (20,33).

The globin domain exhibits an efficient sensor function based on the reactivity of the heme iron atom (56,69). Its structure is a variant of the 3-over-3 helical fold with an extra N-terminal Z-helix and no D-helix (44,63,70,75). Binding of diatomic gaseous ligands causes a conformational change of the sensor domain that is transferred *via* a linker region to the transmitter domain, regulating its activity. A comprehensive model for a full-length GCS has been proposed for *E. coli* diguanylate cyclase DosC (*Ec*DosC) (63), although the precise mechanism of signal transduction within the molecule has still to be elucidated further.

Most known GCS have a transmitter domain mainly consisting of a GGDEF domain with DGC activity. GCS with DGC (or PDE) activity produce (or degrade) cyclic-di-(3',5')-GMP (c-di-GMP), a key second messenger involved in the conversion from a free-living into a sessile-living bacterial population through biofilm formation (23,32,57) and modulation of pathogenic factors (53). Bacteria in a biofilm show resistance to antibiotics and the host immune system and often result in persistent and chronic diseases (16). As such, biofilms are considered an important medical and industrial issue and, consequently, GCS with DGC activity are becoming of increasing scientific interest. Two examples of such biofilm-forming bacteria with a GCS are *Azotobacter vinelandii* and *Bordetella pertussis*.

*Azotobacter vinelandii* is a Gram-negative, alginate-biofilm-producing bacterium, capable of diazotrophic growth and N-fixation in the presence of $O_2$ (48). As such it has economic importance and it is widely used as a research model system. Genomic analysis revealed the presence of a GCS (*Av*GReg) (55,64). *Av*GReg is a 472 residues soluble protein consisting of a 178 residues N-terminal globin sensor domain (*Av*GReg-Gb) and a 170 residues C-terminal GGDEF transmitter domain endowed with a DGC activity.

*Bordetella pertussis* is a Gram-negative, aerobic, biofilm forming bacterial pathogen (9,36,73). It is the causative of pertussis or whooping cough a highly contagious human disease that still causes, yearly, many deaths among children worldwide (World Health

Antioxidants and Redox Signaling
Structural and functional characterization of the globin-coupled sensors of *Azotobacter vinelandii* and *Bordetella pertussis* (DOI: 10.1089/ars.2018.7690)
This paper has been peer-reviewed and accepted for publication, but has yet to undergo copyediting and proof correction. The final published version may differ from this proof.

Organization: http://www.who.int/topics/pertussis/en/). In the *Bordetella pertussis* genome, one GCS with gene regulating function has been identified, namely *Bpe*GReg (3, 4). As *Av*GReg, *Bpe*GReg is a di-domain molecule (475 residues) consisting of a globin-like sensor domain (residues:1-155) covalently attached by a linker region (residues:156-296) to a transmitter domain (residues: 297-475) with DGC activity. This enzymatic activity is regulated by ligand ($O_2$) binding to the sensor domain, product (c-di-GMP) binding to an inhibitory site (RxxD motive in the transmitter domain), and the oligomerization state (mono- di- or tetramer) of the full GCS protein (6,7,50,70). The participation of c-di-GMP in the process of biofilm formation of *Bpe*GReg has been demonstrated *in vivo* (70). The iron bound $O_2$ is stabilized by a TyrB10 and SerE11 residue of the globin sensor domain. Dimerization of this domain involves the G and H helices (7,50).

*Av*GReg and *Bpe*GReg not only merit scientific attention due to their respective economic and medical importance, but a thorough comparison of the structural and functional properties of these two molecules can contribute to a better understanding of the general role of GCSs in the signaling mechanism associated with the formation of bacterial biofilms. We have therefore combined different biochemical and biophysical techniques to unravel the structural-function relationship of these two proteins. The study involves the comparative analysis of the *Av*GReg and *Bpe*GReg full-length molecules, their respective globin domains and some mutants (*Av*GRegYB10F and Cys-mutant *Bp*eReg*). In the latter notation, asterisk indicates the Cys-Ser mutation of Cys16, Cys45, Cys114 and Cys154, needed for crystallization purposes, see Materials and Methods for details. Moreover, the full-length *Av*GReg was for the first time obtained *via in-vivo* folding, which led to a molecule with marked differences in the ligand binding properties than reported earlier for *in-vitro* folded *Av*GReg (from now on referred to as $^{\dagger}$*Av*GReg) (64).

**Results**

*UV/Vis spectroscopy*

The absorbance maxima of the UV/VIS spectra of full-length *Av*GReg and *Bpe*GReg, in different ligation forms are reported in Table 1. The spectra of the 'as purified' forms are typical for low-spin $O_2$-ligated ferrous globins, while those of the reduced forms are characteristic for ferrous high-spin pentacoordination of the heme. The absorbance maxima do not change for the truncated proteins consisting only of the globin domains

(*Av*GReg-Gb and *Bpe*GReg-Gb), nor for the Cys mutant (*Bpe*GReg*) and the YB10F mutant of *Av*GReg (data not shown). Overall these results confirm the presence of a globin domain capable of gaseous ligand binding and they are comparable to what was already reported for GCS in the literature (50,70).

*Resonance Raman spectroscopy*

The resonance Raman (RR) spectra for *Av*GReg(-Gb) and *Bpe*GReg(-Gb) were recorded in the as-purified ($O_2$-bound ferrous) state, and in the dithionite-reduced (deoxy ferrous) state (Fig. 1). The corresponding spectra of *Bpe*GReg* and *Bpe*GReg-Gb* are depicted in Figure S1. The high frequency region (1300-1800 $cm^{-1}$) of the spectrum provides insights on the oxidation ($\nu_4$), coordination ($\nu_3$), and spin ($\nu_2$) states of the heme iron atom (59) (Fig. 1B,D, Table 2). The observed marker frequencies are in accordance with those reported for *Sw*Mb (60,61) and different gas sensor proteins, such as the *Bacillus subtilis* heme-based aerotaxis transducer (*Bs*HemAT) (2), the isolated globin domain of *Ec*DosC (*Ec*DosC-heme) (28), and the globin-coupled histidine kinase from *Anaeromyxobacter sp.* Fw109-5 (*Af*GcHK) (29) (Table 2). They confirm the assignment of the ferrous form of *Av*GReg(-Gb) and *Bpe*GReg to a high-spin pentacoordinated heme site. The as-purified proteins are all in the $O_2$-ligated ferrous form. Interestingly, the RR spectrum of *Bpe*GReg (Fig. 1D,a) reveals partial photolysis of the $O_2$ ligand (two $\nu_4$ bands at 1359 $cm^{-1}$ and 1373 $cm^{-1}$, agreeing with the deoxy and oxy ferrous form). The partial photolysis hampers the analysis of the low-frequency part of the RR spectra of $O_2$-*Bpe*GReg, which will therefore not be considered in the below discussion.

The low frequency region (200-900 $cm^{-1}$) reveals in-plane and out-of-plane vibrational modes of the heme (59). The $\nu_{Fe\text{-}His}$ is observed at 227 $cm^{-1}$ for the ferrous unligated *Av*GReg (Fig. 1A,b). This value is similar to that of ferrous *Bs*HemAT (225 $cm^{-1}$) (2) and *Ec*DosC-heme (227 $cm^{-1}$) (28). The $\nu_{Fe\text{-}His}$ peak broadens and shifts to ~214 $cm^{-1}$ for *Av*GReg-Gb (Fig. 1A,d). For all deoxy ferrous *Bpe*GReg* and *Bpe*GReg-Gb* forms, the $\nu_{Fe\text{-}His}$ mode is observed as a broad peak around 229-233 $cm^{-1}$ (Fig. 1C,b,d, Fig. S1Ab,d). The $\nu_{Fe\text{-}His}$ stretching mode is known to depend on different parameters (2,39,43). The higher $\nu_{Fe\text{-}His}$ mode found in ferrous unligated *Av*GReg and *Bpe*GReg can indicate a stronger H-bonding to the proximal His $N^{\delta}$ nitrogen, less strain on the Fe-His bond, and/or a smaller dihedral angle $\phi$ between imidazole plane and the nearest N(pyrrole)-Fe-N(pyrrole) axis. Thus, in

Antioxidants and Redox Signaling
Structural and functional characterization of the globin-coupled sensors of *Azotobacter vinelandii* and *Bordetella pertussis* (DOI: 10.1089/ars.2018.7690)
This paper has been peer-reviewed and accepted for publication, but has yet to undergo copyediting and proof correction. The final published version may differ from this proof.

keeping with the sensor functionality, the $\nu_{Fe\text{-}His}$ difference observed between *Av*GReg and *Av*GReg-Gb points to an influence of the signaling domain on the heme proximal region of the globin domain. Similarly, the $\gamma_7$ pyrrole bending mode, observed usually between 288 - 313 $cm^{-1}$ in heme proteins and indicative of an out-of-plane distortion of the heme, changes slightly from a sharp peak at 301 $cm^{-1}$ for deoxy *Av*GReg to a broadened peak at 299 $cm^{-1}$ for deoxy ferrous *Av*GReg-Gb (Fig. 1A). This is also found for the deoxy form of horse heart Mb (302 $cm^{-1}$) (25). In both cases, $O_2$ ligation causes a reduction of the out-of-plane distortion (less pronounced $\gamma_7$ mode). A similar trend is observed for the $\gamma_7$ bending modes of *Bpe*GReg(-Gb) (Fig. 1C).

The heme propionate and vinyl modes reveal important information about the stabilization of the heme by the surrounding protein. The vinyl $\delta(C_\beta C_a C_{b2,4})$ bending modes more or less coincide and give rise to broadened peaks around 421, 414 and 417 $cm^{-1}$ for $O_2$-*Bpe*GReg-Gb, $O_2$-*Bpe*GReg* and $O_2$-*Bpe*GReg-Gb*, respectively (Fig. 1C,c, Fig. S3A,a,c). This indicates that the out-of-plane distortions influence each of the pyrrole units in a similar way (68). The increase in wavenumber of this mode for the globin domain compared to the full length domain, indicates an effect of the transmitter domain on the globin domain. This effect was not observed for the *Av*GReg proteins (415 $cm^{-1}$ (Fig. 1Aa,c)). Deoxygenation leads for *Bpe*GReg* and *Bpe*GReg-Gb* to $\delta(C_\beta C_a C_{b2,4})$ bending modes at 412 $cm^{-1}$, whereby the peaks are clearly less broad than in the case of the oxygenated proteins (Fig. 1C, Fig. S1). This means that $O_2$ ligation influences the stabilization of the two vinyl groups in a different way. Again, this effect is far less pronounced in the *Av*GReg case (Fig. 1A).

$O_2$-*Av*GReg and $O_2$-*Av*GReg-Gb display the $\delta(C_\beta C_c C_d)$ propionate bending mode at 381 $cm^{-1}$ and 377 $cm^{-1}$, respectively (Fig. 1Aa,c), while those of $O_2$-*Bpe*GReg-Gb, $O_2$-*Bpe*GReg* and $O_2$-*Bpe*GReg-Gb* are found at 382, 375 and 378 $cm^{-1}$, respectively (Fig. 2C,c, Fig. S1A,a,c). This suggests a moderate to strong electrostatic interaction of the heme propionate groups with the surrounding amino-acid side chains. Interestingly, the $\delta(C_\beta C_c C_d)$ mode is found at 363 $cm^{-1}$ for ferrous *Av*GReg, and 380 $cm^{-1}$ for ferrous *Av*GReg-Gb, respectively. The former low value reflects the pronounced effect of the second domain on the heme surrounding upon ligand binding. While this mode is still clearly detectable for the deoxy ferrous state of *Av*GReg(-Gb) (Fig. 1A,b,d), the $\delta(C_\beta C_c C_d)$ mode

can only be weakly observed for deoxy ferrous *Bpe*GReg-Gb (Fig. 1Cd, small peak at 379 $cm^{-1}$).

For the *in vivo* folded $O_2$-*Av*GReg and $O_2$-*Av*GReg-Gb, two $\nu_{Fe-O2}$ modes were found (Fig. 1Ab,d, Table 2). The first mode is located at 563 $cm^{-1}$ (561 $cm^{-1}$), while the second mode is located at 573 $cm^{-1}$ (see Fig. S2, for a details of this spectral region in the RR spectrum of $O_2$-*Av*GReg). The 573 $cm^{-1}$ mode is similar to the one observed for other globins, such as Mb which show $\nu_{Fe-O2}$ around 570 $cm^{-1}$ (12,24,27,58). Lower Fe-$O_2$ stretching modes of 557-560 $cm^{-1}$ have been found for the oxygenated forms of *Bs*HemAT (2) and *Af*GcHK (29) (Table 2). In this respect, previous studies on *Mycobacterium tuberculosis* (74) and *Chlamydomonas eugametos* 2/2Hbs (11) indicate that the low $\nu_{Fe-O2}$ mode is related to a strong hydrogen bond between the bound $O_2$ molecule and residue TyrB10. As such, this low $\nu_{Fe-O2}$ mode suggests a strong stabilization of the bound $O_2$ through hydrogen bonding in *Av*GReg, while the 573 $cm^{-1}$ indicates the co-existence of a more open configuration in which the $O_2$ is not stabilized. For the oxygenated *Bpe*GReg* variants, only a $\nu_{Fe-O2}$ mode in the 556-560 $cm^{-1}$ region is found (Table 2, Fig. 1, Fig. S1), indicating that the $O_2$ ligand is strongly hydrogen bonded to distal amino-acids with no open conformation present. This will be shown to correlate with the kinetics data. A very recent FTIR study on the CO-ligated ferrous *Bpe*GReg and its Tyr43Phe variant revealed that one of the CO-bound conformers is strongly hydrogen-bonded to the distal Tyr(43)B10, in line with the here observed H-bonding of the $O_2$ ligand (51).

In earlier work, we already performed RR analyses on $^{\dagger}$*Av*GReg(-Gb) (64). While the RR data obtained in both studies are similar for the globin domain of the protein, the RR and electron paramagnetic resonance data of $^{\dagger}$*Av*GReg showed the protein to be in the ferric form due to the *in-vitro* refolding. Figure S3 (supplementary material) shows the optical absorption and RR data for *Av*GReg oxidized with ferricyanide. It shows that (partial) oxidation of the protein can be obtained chemically, but that it also leads to partial denaturation of the protein as can be derived from the optical absorption peak at 646 nm. The spectra in Figure S3 for oxidized *Av*GReg agree with those previously obtained for $^{\dagger}$*Av*GReg, where also signs of partial denaturation were found (64).



Antioxidants and Redox Signaling
Structural and functional characterization of the globin-coupled sensors of *Azotobacter vinelandii* and *Bordetella pertussis* (DOI: 10.1089/ars.2018.7690)
This paper has been peer-reviewed and accepted for publication, but has yet to undergo copyediting and proof correction. The final published version may differ from this proof.

Antioxidants and Redox Signaling
Structural and functional characterization of the globin-coupled sensors of *Azotobacter vinelandii* and *Bordetella pertussis* (DOI: 10.1089/ars.2018.7690)
This paper has been peer-reviewed and accepted for publication, but has yet to undergo copyediting and proof correction. The final published version may differ from this proof.

*Ligand binding kinetics on AvGReg proteins*

*Av*GReg proteins and the *Av*GReg YB10F mutant were characterized in terms of the CO and $O_2$ binding equilibria and their kinetics as described in Materials and Methods. In the whole CO concentration range explored in the flash-photolysis experiments, the time courses of the CO binding to *Av*GReg can be described by a single exponential, allowing the use of a minimum reaction mechanism (Scheme 1, Materials and Methods (64)). The value of the kinetic parameter that defines CO binding ($k'_{CO}$ = (0.48 ± 0.01) x $10^6$ $M^{-1}$ $s^{-1}$) is very similar to the value reported for *Sw*Mb (Table 3; Fig. 2). Only a minor influence is noticed of the protein truncation or YB10F mutation. However, the other GCSs characterized to date show a very moderately (*Bs*HemAT) to significantly lower (*Ec*DosC and *Af*GcHK) CO association rate constant (Table 3).

The results of the flash-photolysis $O_2$/CO competition experiment can be described with a second order reaction mechanism (see Materials and methods, Scheme 2). The $O_2$ association/dissociation rate constants of *Av*GReg, as well as the constant for CO dissociation from *Av*GReg (Table 3; Fig. 2C,D), have been determined using Equations 1 and 2 (see Materials and methods). Interestingly, stopped-flow measurements reveal the presence of a second phase in the $O_2$/CO replacement mechanism (Table 3; Fig. 2B). Therefore, we can conclude that *Av*GReg is characterized by a fast $O_2$ binding ($k'_{O2}$ = (12.2 ± 1.5) x $10^6$ $M^{-1}$ $s^{-1}$) and two $O_2$ dissociation constants ($k_{O2}$ = (1732 ± 377) $s^{-1}$ and $k_{O2}$ = (0.53 ± 0.05) $s^{-1}$).

The $O_2$ association and dissociation rate constants we present here for the *Av*GReg differ significantly from the ones measured previously for the *in vitro* refolded protein $^{\dagger}$*Av*GReg (Table 3). In particular, $^{\dagger}$*Av*GReg appears to release dioxygen 160 times slower (high $k_{O2}$) and 1.3 times faster (low $k_{O2}$).

While two distinct $k'_{O2}$ values were measured for *Af*GcHK (29), a biphasic $O_2$ dissociation was observed for *Bs*HemAT (75) as for *Av*Greg (Table 3). A difference of more than 200 fold is revealed when comparing the higher $K_d$ values of *Av*GReg and *Af*GcHK, while the lower $K_d$ values are in the same order of magnitude for the two GCSs. This indicates the presence of an extremely stable Fe-$O_2$ complex in both cases. In contrast, we find that the higher $K_d$ value of *Av*GReg and *Bs*HemAT are in the same order of magnitude, while the lower $K_d$ of *Av*GReg is 100 times smaller than that of *Bs*HemAT. The latter

observation highlights the very high $O_2$ affinity of *Av*GReg, being the highest among the other globin sensors characterized to date, suggesting that it can be (and remain) activated in the presence of traces amounts of $O_2$.

A likely explanation of these results lies in the observation of two $\nu_{Fe-O2}$ modes for $O_2$-ligated *Av*GReg in solution, linked to an *open* and *closed* conformation for the $O_2$ stabilization, responsible for the two dissociation constants, similarly as for *Bs*HemAT (75). Within this model, when the globin domain is in the *open* conformation, $O_2$ is less stabilized inside the heme pocket, allowing a more efficient diffusion of CO from the outer environment, and faster $O_2$ displacement. On the other hand, in the *closed* conformation, $O_2$ is firmly bound in the heme pocket, and well protected from the solvent. The competition between $O_2$ and CO is impaired, thus $O_2$ displacement is significantly slower. The results for *Av*GRegYB10F indicate that Tyr(44)B10 plays an important role in this regulation (Table 3, Fig. S4). Not only does the fastest $O_2$ dissociation rate increase with an order of magnitude upon mutation, the dissociation rate from the *closed* confirmation increases with a factor of ~300.

*Ligand binding kinetics on Bordetella pertussis proteins*

The ligand binding parameters for CO and $O_2$ binding to *Bpe*GReg and *Bpe*GReg-Gb, are summarized in Table 3 and Fig. 3. Interestingly, the CO binding reactions of *Bpe*GReg and the isolated *Bpe*GReg-Gb show a different decay. The double exponential rebinding to *Bpe*GReg is defined with $k'_{COfast}$ = 0.60 $\mu M^{-1}$ $s^{-1}$ and $k'_{COslow}$ = 0.01 $\mu M^{-1}$ $s^{-1}$, while the rate constant of the *Bpe*GReg-Gb single exponential reaction is $k'_{CO}$ = 0.11 $\mu M^{-1}$ $s^{-1}$. The explanation for this difference must be related to the presence of the transmitter domain, though we believe it goes beyond the mere structural effect of the absence/presence of this domain, as no major modification of the heme environment can be ascribed to the isolated globin domain. Considering also the dimerization process, we confirm the data by Rivera *et al*. (50) that the intra- and intermolecular interactions influence the ligand binding capabilities and, therefore, result in this CO affinity difference. Surprisingly, recent FTIR of *Bpe*GReg-Gb and *Bpe*GReg showed three CO stretches in both proteins, corresponding to an open and a closed (H-bonded) conformation and a pH-dependent conformer stabilized by structural water (51).

Antioxidants and Redox Signaling
Structural and functional characterization of the globin-coupled sensors of *Azotobacter vinelandii* and *Bordetella pertussis* (DOI: 10.1089/ars.2018.7690)
This paper has been peer-reviewed and accepted for publication, but has yet to undergo copyediting and proof correction. The final published version may differ from this proof.

The $O_2$/CO competition studies and the $O_2$ association/dissociation rate constants of *Bpe*GReg have been determined as for *Av*GReg. With $k'_{O2}$ = 24.02 $\mu M^{-1}$ $s^{-1}$ and $k_{O2}$ = 4.0 $s^{-1}$ (Table 3), *Bpe*GReg is capable of selective and more efficient $O_2$ binding when a gas mixture is present, as is also the case for myoglobin (1). Moreover, the low $K_d$ values for $O_2$ ($K_d$ = 0.17 µM) indicate that this sensor will be saturated with $O_2$ in physiological conditions. This is in line with the RR data that reveal only one $\nu_{Fe-O2}$ mode agreeing with a strong hydrogen bonding and thus stabilization of the dioxygen ligand. Despite the fact that the reported $k'_{O2}$ from Wan *et al*. (70) is lower, the results are in accordance with the reported transmitter domain activation *via* $O_2$ binding to the sensor domain (70). Indeed, the very high affinity of the full-length *Bpe*GReg suggests that this characteristic ensures a stable promotion of the *Bpe*GReg DGC activity, resulting in the typical chronic infection-related biofilm persistence (6,7,50,70).

*Diguanylate cyclase activity of AvGReg*

We measured and analyzed the DGC activity of *AvGReg* to complement the already published data on *Bpe*GReg (7,70). By means of an optimized DGC activity assay, we could collect reproducible time point series within few seconds from time zero to confidently determine the initial reaction rate. We tested numerous substrate concentrations, which revealed a high sensitivity of $O_2$-*Av*GReg to product inhibition, as already reported for *Bpe*GReg and *Ec*DosC (28, 70). To avoid bias due to this effect, we determined the enzyme specificity constant (calculated as $k_{cat}/K_m$) at GTP concentrations where no product inhibition was detected as described in Material and Methods (Fig. 4) and no cooperativity was seen.

For the oxygenated form of the *in vivo* folded *Av*GReg, the reaction reached completion after 20 minutes for all the substrate concentrations used (20 to 65 µM GTP) (data not shown), yielding a $k_{cat}/K_m$ value of (1.13 ± 0.13) x $10^4$ $M^{-1}$ $s^{-1}$. $O_2$-*Bpe*GReg shows a 66 fold lower enzyme specificity as published by Burns *et al* ($k_{cat}/K_m$ = 0.17 x $10^3$ $M^{-1}$ $s^{-1}$) (6) with completion reached after 30 minutes, while *Ec*DosC is characterized by a high autoxidation rate that hindered the estimation of the exact turnover number (28). The ferrous unligated form of *Av*GReg was also assayed for DGC activity. Comparison of the $O_2$-*Av*GReg and unligated *Av*GReg catalyzed reactions showed that in the latter case c-di-GMP synthesis is 50% decreased (Fig. 4), as previously reported also for *Bpe*GReg and *EcDosC*

(28,70). These results confirm the role of $O_2$ as DGC reaction trigger for this class of GCSs. Considering that *A. vinelandii* does not grow anaerobically and the very high $O_2$ affinity of *Av*GReg, it is likely that in physiological condition the *Av*GReg sensor is in the $O_2$-bound active state already in the presence of traces amounts of $O_2$.

*Tertiary and quaternary structures of AvGReg-Gb and BpeGReg-Gb**

The ferric aquo-met form of *Av*GReg-Gb and *Bpe*GReg-Gb* crystal structures have been determined at 2.83 Å and 3.20 Å resolution, respectively (two molecules per asymmetric unit, referred to as A and B in both cases). The final *Av*GReg-Gb model consists of 258 amino acids; no electron density is observed for residues 48-67 and 46-69 in chains A and B, respectively (B-C-E region). The refined *Bpe*GReg-Gb* structure comprises 306 amino acids; only residues 57-63 in chains B (C-E loop) show poor electron density. Data collection and refinement statistics are reported in Table 4.

The overall fold of *Av*GReg-Gb and *Bpe*GReg-Gb* conform to the modified globin fold typically found for GCS sensor domains (44,63,75) and protoglobin (40,45,46), consisting of 8 helices which, according to the classical globin nomenclature, have been named in alphabetical order from A to H, with a Z helix preceding the A at the N-terminus and the D helix absent (Figs. 5A,B). The two *Av*GReg-Gb and *Bpe*GReg-Gb* structures superimpose well, with a root mean squared deviation (rmsd) of ~1.3 Å over 126 Cα atom pairs, with structural differences localized at the N-terminal region (including the Z helix), in the B-E region, in the EF and GH loops (Fig. 5C).

Overall, two major features, both associated to the heme pocket, uniquely characterize *Av*GReg-Gb. On the heme-proximal side *Av*GReg-Gb exhibits one of the longest F-helix seen in globins (23 residues); this is due to the fact that the N-terminus of the F helix contains one more turn at the expense of the C-terminal turn of the E helix (Fig. 5A,C). On the heme-distal side the structural disorder at the B-C-E region (in both the A and B chains) results in the unwinding of almost the whole B-helix (Fig. 5A). The B-C-E region is instead well structured in *Bpe*GReg-Gb* (Figs. 5B,C).

The *Av*GReg-Gb and *Bpe*GReg-Gb* monomers assemble in homodimers with the interface residues belonging to the Z, G, and H helices of both A and B chains (Fig. 6A,B). Thus, the dimerization interface has a four α-helical G-H bundle as the core region (including 11 H-bonds and 7 salt bridges for *Av*GReg-Gb, and 11 H-bonds and 16 salt

bridges for *Bpe*GReg-Gb*), while the adjacent Z helices provide mostly van der Waals interactions. The dimeric assembly observed in *Av*GReg-Gb and *Bpe*GReg-Gb* is similar to those found in *Gs*GCS[162] (PDB code: 2W31) (44), *Bs*HemAT (PDB codes: 1OR4, 1OR6) (75), *Ec*DosC (PDB code: 4ZVA, 4ZVB) (63), and in *Ma*Pgb (PDB codes 2VEB, 2VEE) (40). However, the dimeric interface surface area can vary significantly: it is large for *Ma*Pgb (~2,100 Å$^2$), *Bs*HemAT (~1,800 Å$^2$) and *Gs*GCS[162] (~1,700 Å$^2$), medium for in *Ec*DosC (~1,300 Å$^2$) and *Av*GReg-Gb (1,304 Å$^2$), and only 1,042 Å$^2$ for *Bpe*GReg-Gb*.

Furthermore, the precise orientation of the A/B subunits in the dimer is not the same in different GCS proteins. Indeed, when the *Av*GReg-Gb A chain is superimposed to that from the other GCSs, the match with the B chain is good for *Bpe*GReg-Gb* and *Ec*DosC, while the *Bs*HemAT B chain is rotated by ~20°, and *Gs*GCS[162] and *Ma*Pgb by ~30°, around an axis approximatively orthogonal to the G-H helices. Strikingly, a similar (albeit more pronounced, ~60°) different orientation of the subunits of the dimer has been found in another *Bpe*GReg-Gb* crystal form (same spacegroup *C*2, but different unit cell), determined at 1.55 Å resolution (*Bpe*GReg-Gb*-2) (Table 4). This second quaternary structure is symmetrical around a crystal axes, covers a contact surface of 1,305 Å$^2$ (similar to *Av*GReg-Gb and *Ec*DosC) with 14 hydrogen bonds and 10 salt bridges, and involves the Z, G, and H helices, and the CE corner (Fig. 6C,D).

It should be noted that the different dimerization mode cannot be ascribed to a different structure of the interfacing monomers, since the *Bpe*GReg-Gb* and *Bpe*GReg-Gb*-2 structures don't show significant deviations if compared monomer by monomer (rmsd values ranging between 0.50 Å and 0.80 Å, over 138-145 Cα pairs). The different quaternary assembly is most likely responsible for the minor structural deviations observed at the N-terminus of the E helix, in the FG, G, GH, and H regions between the *Bpe*GReg-Gb* and *Bpe*GReg-Gb*-2. In particular, the C-terminal His155 residue, buried at the dimeric interface in *Bpe*GReg-Gb *, is solvent exposed in *Bpe*GReg-Gb*-2 and interacting with an additional heme group (probably released in solution by a fraction of *Bpe*GReg-Gb*) which becomes hexacoordinated between the end of two H-helices at the top of the dimeric interface (Fig. 6E,F).



Antioxidants and Redox Signaling
Structural and functional characterization of the globin-coupled sensors of *Azotobacter vinelandii* and *Bordetella pertussis* (DOI: 10.1089/ars.2018.7690)
This paper has been peer-reviewed and accepted for publication, but has yet to undergo copyediting and proof correction. The final published version may differ from this proof.

*Heme proximal side*

*Av*GReg-Gb and *Bpe*GReg-Gb* share a very similar heme pocket proximal side, due to a very high sequence similarity in this protein region. The proximal heme pocket is lined by residues Ile(97)F4, Ile(100)F7, Ile(104), Ile(106), Val(111)G4, and Met(154)H17 in *Av*GReg-Gb, and Val(95)F4, Val(98)F7, Ile(102), Ile(104), Val(109)G4, and Met(153)H17 in *Bpe*GReg-Gb*, which surround and mostly contact the porphyrin ring.

Both *Av*GReg-Gb and *Bpe*GReg-Gb* show a loose coordination bond between the Fe atom and the proximal His residue with Fe–His(101)F8 NE2 distance of 2.39 Å and 2.50 Å in the A and B monomers of *Av*GReg-Gb, and Fe–His(99)F8 distance of 2.10 Å and 2.29 Å in A and B chains of *Bpe*GReg-Gb*. In *Av*GReg-Gb and *Bpe*GReg-Gb* the F8 imidazole ring lies in a staggered azimuthal orientation relative to the heme pyrrole N-atoms in chain A, and it is eclipsed in chain B along the direction of the heme pyrrole NA-NC atoms in *Av*GReg-Gb and NB-ND in *Bpe*GReg-Gb* (Fig. 7A). In the *Bpe*GReg-Gb*-2 His(99)F8 stabilizes the heme iron atom with a distance of 2.20 Å in chain A and 2.14 Å in chain B, being always eclipsed along the direction of the heme pyrrole NB and ND atoms.

*Heme distal side*

The heme distal side of *Av*GReg-Gb and *Bpe*GReg-Gb* varies considerably, but both reveal a high conformational flexibility of the B-C-E region. In *Av*GReg-Gb the heme distal pocket residues Tyr(42)B8, Phe(43)B9, Tyr(44)B10, and Leu(70)E11 surround a heme-ligated water molecule (2.81 Å and 3.32 Å in the A and B chains, respectively), which is not stabilized by any polar interaction provided by the protein (Fig. 7A). It should be noted, however, that part of the heme-distal site corresponding to the B-C-E region (residues 48-67 and 46-69 in chain A and chain B, respectively), could not be modeled due to the low connectivity of the experimental electron density map. In particular, this disordered region involves the C-terminal end of the B-helix, which in *Av*GReg-Gb appears to be almost completely unwound (Fig. 5A). As a consequence, Tyr(44)B10, a conserved residue usually involved in ligand stabilization in GCS proteins, is too far to H-bond the heme-bound water molecule (Fig. 7A). The same considerations hold for the nearby Tyr(42)B8, an amino acid which is instead specific of *Av*GReg-Gb and few others GCSs (19). However, both Tyr residues point their hydroxyl groups towards the interior of the distal site and, therefore, could be involved in ligand stabilization in the context of a structured B-C-E region.

Antioxidants and Redox Signaling
Structural and functional characterization of the globin-coupled sensors of *Azotobacter vinelandii* and *Bordetella pertussis* (DOI: 10.1089/ars.2018.7690)
This paper has been peer-reviewed and accepted for publication, but has yet to undergo copyediting and proof correction. The final published version may differ from this proof.

Conformational disorder at the BE distal site region has been previously reported in GCSs and other globins, and, in some cases, associated to functional roles. For instance, in GCSs and related proteins (*i.e.* protoglobin) disorder in this region has been associated to multiple conformations of specific residues whose side-chain orientations in the heme-distal site depend on the ligation state of the heme-Fe atom (40,44,45,46,75). However, in *Av*GReg-Gb the disordered region is delimited by residues Gly(40)B6-Pro(41)B7 on one side and Gly(68)E9 on the other, which are specific for *Av*GReg-Gb and not conserved in other GCSs (19,44).

The *Bpe*GReg-Gb* heme iron atom coordinates to a water molecule (at 3.06 Å in the A chain and at 2.90 Å in the B chain) at the distal site, which is not stabilized by any interaction with the amino acids facing the distal site. In particular, Tyr(43)B10 is pointing its hydroxyl group towards the exterior of the distal site. The distal side residues are hydrophobic (Phe(42)B9, Leu56, Val(61)E3, Leu(65)E7, Met(69)E11) and well defined in the A chain of the dimer, while in the B chain the C-E region (residues 57-60) is partly disordered (Fig. 7B). Interestingly, the second crystal form, *Bpe*GReg-Gb*-2, shows an Fe-coordination state at the distal site that differs in the A and B chains and from the *Bpe*GReg-Gb* crystal form: the heme-Fe is loosely hexacoordinated to Tyr(43)B10 (3.11 Å) in chain A, (Fig. 7C) and to an imidazole molecule (2.12 Å), probably originating from the purification protocol, in chain B, with Tyr(43)B10 swinging out from the distal site due to steric repulsion caused by the imidazole ligand (Fig. 7D). Overall, we can conclude that the different dimerization mode of *Bpe*GReg-Gb*-2 has an impact in the distal site geometry reshaping, with Tyr(43)B10 able to point inwards and outwards, in keeping with the previously proposed mechanism whereby the globin domain dimerization leads to conformation(s) of the distal pocket that adjust the position of the hydrogen bonding residues involved in $O_2$ dissociation kinetics (50). Interestingly, the distal site swinging movement of TyrB10 has been suggested as the mechanism of $O_2$ stabilization for other GCSs, as *Bs*HemAT (75) and *Ec*DosC (63).

In *Bpe*GReg-Gb* the heme group's propionates are not interacting with Lys(64)E6 at the distal site, nor with Lys(94)F3 at the proximal site (Fig. 7A), while in the *Bpe*GReg-Gb*-2 structure only a loose interaction is present with Lys(64)E6 (Fig. 7C,D).

Antioxidants and Redox Signaling
Structural and functional characterization of the globin-coupled sensors of *Azotobacter vinelandii* and *Bordetella pertussis* (DOI: 10.1089/ars.2018.7690)
This paper has been peer-reviewed and accepted for publication, but has yet to undergo copyediting and proof correction. The final published version may differ from this proof.

**Discussion**

The *A. vinelandii* and *B. pertussis* are highly interesting bacterial systems. Indeed, *A. vinelandii* fixes $N_2$ in the presence of $O_2$, a unique metabolic feature that renders it particularly interesting for industrial applications whereas *B. pertussis* is a highly contagious human pathogen that still causes many deaths worldwide and is, therefore, of considerable medical interest. In addition, the GCS of both systems are involved in biofilm formation. In this respect, their characterization, here presented, is significant for a more detailed understanding of the control that the sensors might exert on biofilm formation.

The combination of biochemical techniques applied in this study provides complementary pictures of *Av*GReg and *Bpe*GReg functional and structural behaviors. We performed our experiment on *in vivo* folded full-length proteins. It is important to note that in the previously published study on *Av*GReg and *Av*GReg-Gb, both proteins had been purified from inclusion bodies, followed by *in vitro* refolding (64). The high level of agreement between our data and the optical and RR spectra of the *in vitro* refolded *Av*GReg-Gb is an indication of the reliability of the refolding method when applied to the globin domain alone. In contrast, the discrepancies detected between *in vivo* folded *Av*GReg and that purified from inclusion bodies strongly suggest that the presence of the second (transducer) domain may hamper a correct *in vitro* refolding process.

We showed that both the *in vivo* folded *Av*GReg and *Bpe*GReg sensors are oxygenated when purified and pentacoordinated when the deoxy ferrous species is produced through dithionite reduction. Additionally, based on our enzymatic *in vitro* assays and the literature, we proved that $O_2$ binding triggers c-di-GMP biosynthesis and that $O_2$-*Av*GReg and $O_2$-*Bpe*GReg are the catalytically competent forms. $O_2$-*Av*GReg and $O_2$-*Bpe*GReg display a high sensitivity to product inhibition confirming the literature (70). For $O_2$-*Av*GReg and $O_2$-*Bpe*GReg a $k_{cat}/K_m$ value of $1.13 \pm 0.13 \times 10^4$ $M^{-1}$ $s^{-1}$ (reported here) and $0.17 \times 10^3$ $M^{-1}$ $s^{-1}$ (6,7) was obtained, respectively. The RR measurements indicate that the heme pocket of the fully oxygenated proteins are well structured, with moderate to strong electrostatic interactions of the heme propionate groups with the surrounding amino-acid side chains and the $O_2$ molecule tightly bound to the heme-Fe for all forms and an additional more open distal heme-pocket site for $O_2$-*Av*GReg. These data are confirmed by the recently published structure of the oxygenated form of *Bpe*GReg-Gb (structure not yet

Antioxidants and Redox Signaling
Structural and functional characterization of the globin-coupled sensors of *Azotobacter vinelandii* and *Bordetella pertussis* (DOI: 10.1089/ars.2018.7690)
This paper has been peer-reviewed and accepted for publication, but has yet to undergo copyediting and proof correction. The final published version may differ from this proof.

released by PDB), where $O_2$ is described as tightly bound to the $Fe^{2+}$ and H-bonded to Tyr(43)B10, and Lys(64)E6 forms a hydrogen bond with heme propionate (51).

The combination of kinetics measurements and the structural data suggest mechanisms for protein activation and signal transduction. In the case of *Av*GReg the kinetics measurements reveal a fast $O_2$ association ($k'_{O2}$ = 12.2 x $10^6$ $M^{-1}$ $s^{-1}$) and a biphasic $O_2$ dissociation, characterized by fast and slow rates ($k_{O2}$ = 1732 and 0.53 $s^{-1}$, respectively). Among GCSs a biphasic $O_2$ dissociation has been reported only for *Bs*HemAT (75). The higher $K_d$ for $O_2$ is in the same order of magnitude for the *Av*GReg and *Bs*HemAT, while the lower $K_d$ highlights the very high $O_2$ affinity of *Av*GReg, being the highest among the other globin sensors characterized to date (see Table 3), suggesting that it can be activated in the presence of traces amounts of $O_2$. The crucial role of Tyr(44)B10 is highlighted by the binding kinetics study of the YB10F mutant which shows a significant increase of $O_2$ dissociation rate, for both the fast and slow rates (Table 3). Specific high affinity $O_2$ binding (needed for sensing, transport, and storage) requires significant deviation from the sliding scale rule, which predict that, although the equilibrium dissociation constants ($K_d$) can vary a lot, the ratios for NO:CO:$O_2$ binding are roughly the same, namely 1:~$10^3$:~$10^6$ when the proximal ligand is a histidine and the distal site is apolar (66). Indeed, data reported for GCSs (including *Bp*eGReg) show that, in general, CO affinity is higher than $O_2$, but that the $K_D(O_2)/K_D(CO)$ ratio is much smaller than that predicted by the sliding scale rule due to a preferentially lower $K_D(O_2)$ associated with hydrogen bonding stabilization of the $O_2$ molecule into the distal site (66).

Within this picture the biphasic behavior for *Av*GReg $O_2$ dissociation, measured by flash-photolysis $O_2$/CO competition, can be explained by the presence of two different *Av*GReg conformations (*open* and *closed*, respectively) responsible for the two dissociation rate constants. More precisely, when the globin domain is in the *closed* conformation, $O_2$ would be firmly bound in the heme pocket and well protected from the solvent. As a result, the competition between $O_2$ and CO would be hampered and $O_2$ displacement significantly slower. On the contrary, when the protein is in the *open* conformation, $O_2$ would be less stabilized within the heme pocket, thus allowing a more efficient diffusion of CO from the outer environment and faster $O_2$ displacement. Both conformations are in keeping with the RR measurements on the fully oxygenated ferrous *Av*GReg. All in all, the

crystal structure of the *Av*GReg-Gb ferric form reveals that the B-C-E region can undergo to structural disorder, probably favoured by the Gly-rich sequence at the BE region boundaries (not present in other GCSs), and this protein flexibility is compatible with the presence of an *open* conformation. From RR and kinetics follows that there is a second more closed (and probably more rigid) conformation that is not populated in the crystals. This closed conformation involves Tyr(44)B10.

Furthermore, the presence of the transmitter domain in the full-length *Av*GReg relaxes the heme proximal coordination when compared to the isolated *Av*GReg-Gb sensor domain. Indeed, the aquo-met crystal structure is in keeping with the RR measurements on the ferrous unligated protein, indicating a staggered conformation of the proximal His(127)F8 side chain and, therefore, a higher strain on the Fe-His bond for the isolated globin domain relative to the full-length protein. Such relaxation at the F-helix proximal His(127)F8 may be also part of the signal transduction mechanism between domains upon $O_2$ binding.

In contrast to *Av*GReg, no dramatic change in the sensor domain of *Bpe*GReg can be ascribed to the absence/presence of the transmitter domain. Indeed, the RR spectra measured on *Bpe*GReg-Gb and *Bpe*GReg (and their *Bpe*GReg-Gb* and *Bpe*GReg* Cys-mutants) are very similar. This suggest that the signal transduction mechanism for the *Bpe*GReg globin domain activation involves structural modifications in protein regions far from the heme pocket. The measured $k'_{O2}$ and $k_{O2}$ values suggest that *Bpe*GReg is capable of selective and more efficiently binding $O_2$ when a gas mixture is present, as is also the case for myoglobin (1). The low $K_d$ ($O_2$) values indicate that, under physiological conditions, the sensor will permanently bind $O_2$. A biphasic behavior for $O_2$ dissociation, as seen for *Av*GReg, is not recorded for *Bpe*GReg, in line with the RR observation of only one (*closed*) conformation for the stabilization of the distal $O_2$ ligand. However, flash photolysis experiments indicate that the CO binding kinetics differs between the isolated *Bpe*GReg-Gb (one exponential) and the full-length *Bpe*GReg (two exponential). This result proves that the overall protein dynamicity changes when the transmitter domain is present, probably due to the presence of structural interactions between sensor and transmitter domains, likely at the oligomerization interface, necessary for the signal transduction process as also seen by Rivera et al (50).

Antioxidants and Redox Signaling
Structural and functional characterization of the globin-coupled sensors of *Azotobacter vinelandii* and *Bordetella pertussis* (DOI: 10.1089/ars.2018.7690)
This paper has been peer-reviewed and accepted for publication, but has yet to undergo copyediting and proof correction. The final published version may differ from this proof.

Finally, the crystal structure of the aquo-met form of *Bpe*GReg-Gb* shows that the water ligand is not stabilized by any distal residue, the Tyr(43)B10 hydroxyl group is pointing away from the heme distal side, and the propionates are not interacting with the protein. These data provide a complementary picture of the recently published $O_2$-bound structure (PDB code: 6M9A) (51) where, instead, the strong $O_2$-binding to Tyr(43)B10 is coupled with heme distortion, interaction between Lys(64)E6 and the heme propionate, and interaction between Ser(68)E10 and Tyr(43)B10 through a distal water molecule, not present in the *Bpe*GReg-Gb* aquo-met form. Thus our data support the proposed mechanism that differences in ligation state at the distal side is potentially propagated through interactions with residues on the E helix, allowing for signaling to the DGC output domain. Furthermore, a second crystal form of ferric *Bpe*GReg-Gb* reveals the presence of two possible dimerization modes, both based on the G-H helical bundle. The first dimerization mode is that typically found in GCSs, the second differs by a rotation of 60° between monomers and is stabilized/forced by the presence of an extra heme molecule, probably due to a somewhat higher heme availability in solution at the more alkaline crystallization condition used (see Material and Methods, condition 2), covalently linking two His residues (His155) at the end of the H helices (the region which is linked to the middle domain of the full-length protein). Although this dimerization mode could be classified as a crystallization artifact, it clearly demonstrates that the G-H surface of a monomer is intrinsically characterize by high plasticity, being able to face, fit and bind its counterpart in more than one way. The different dimerization mode is also associated with a different distal site organization, with Tyr(43)B10 swinging in and out the distal site. Thus, a transmission mechanism through a partial rotation at the G-H interface is conceivable, whereby a different relative position of the H-helices upon ligand binding would directly affect the following middle domain and/or affect the global oligomerization state of the full-lengh protein (dimer with low diguanylate cyclase activity *vs* tetramer with high activity) (51).

Our *in vitro* data on DGC activity in *Av*GReg demonstrate that $O_2$-binding to *A. vinelandii* GCS triggers c-di-GMP biosynthesis, as described for *B. pertussis* GCS (20,33,51,70). In bacteria, C-di-GMP is an essential second messenger involved, *in vivo*, in the regulation (translational and post-translation) of motility, exo-polysaccharide production and biofilm

formation (26,34,49,52). Thus $O_2$ binding to GCS as *A. vinelandii* and *B. pertussis*, increases c-di-GMP production and activates biofilm formation.



Antioxidants and Redox Signaling
Structural and functional characterization of the globin-coupled sensors of *Azotobacter vinelandii* and *Bordetella pertussis* (DOI: 10.1089/ars.2018.7690)
This paper has been peer-reviewed and accepted for publication, but has yet to undergo copyediting and proof correction. The final published version may differ from this proof.

**Innovation**

Biofilms are considered an important medical and industrial issue and, consequently, GCS with DGC activity are becoming a class of enzymes of increasing scientific interest. This paper extends the knowledge on the GCS proteins. It provides a comprehensive biochemical and structural characterization of *A. vinelandii* and *B. pertussis* $O_2$ sensors involved in the control of biofilm formation and biofilm maintenance through production of the c-di-GMP second messenger.

**Materials and Methods**

*Cloning, expression, mutagenesis and protein purification*

Full-length *Av*GReg (472 residues) and its N-terminal globin domain *Av*GReg-Gb (residues 1-170) were amplified by PCR, and cloned into the pBAD-a vector as previously described (14,47,64). In addition, for the *Av*GRegYB10F variant, Tyr(44)B10 was mutated into Phe using the QuickChange™ site-directed mutagenesis method (Stratagene) (15). All were expressed as N-terminal His-tagged proteins in *E. coli* TOP10 cells (Invitrogen) (14,47) and purified from the soluble fraction using affinity chromatography. This procedure is very different from the one used to obtain $^{\dagger}$*Av*GReg in (64). In that case, the procedure involved the purification of the expressed, denatured proteins from inclusion bodies, with a subsequent *in vitro* folding in the presence of hemin. This approach deviates significantly from the here presented method based on *in-vivo* folding of the proteins in *E. coli* followed by affinity purification.

Full-length *Bpe*GReg (475 residues) and its N-terminal globin domain (*Bpe*GReg-Gb) (residues 1-169) were amplified by PCR and cloned into the pET23-a vector using NdeI and XhoI restriction sites. The C-terminal His-tagged fusion proteins were expressed in *E. coli* BL21(DE3)pLysS (Invitrogen) as done for the *Av*GReg proteins (14,47). To prevent aggregation during the crystallization process, four out of six cysteine residues present in the globin domain (Cys16, Cys45, Cys114, Cys154) were mutated into Ser using the QuickChange™ site-directed mutagenesis method (Stratagene) (15). The selection for the Cys residue to be mutated was done based on the *in silico* modelling of *Bpe*GReg-Gb obtained by using the I-TASSER server (72). The mutated proteins are further termed and

Antioxidants and Redox Signaling
Structural and functional characterization of the globin-coupled sensors of *Azotobacter vinelandii* and *Bordetella pertussis* (DOI: 10.1089/ars.2018.7690)
This paper has been peer-reviewed and accepted for publication, but has yet to undergo copyediting and proof correction. The final published version may differ from this proof.

*Bpe*GReg* (full length molecule) and *Bpe*GReg-Gb* (globin domain). The *Av*GReg proteins were kept in 50mM Tris-HCl pH 7.5, 50mM NaCl, 10mM $MgCl_2$ and 5% glycerol, whereas the *Bpe*GReg proteins were kept in 20mM Tris-HCl pH 8, 50mM NaCl and 40% glycerol. Both the globin domains were kept in 50 mM Tris-HCl pH 8.5, 10 mM NaCl and 0.5 mM EDTA.

*UV/Visible absorption spectroscopy*

The optical absorption measurements were obtained by using a Varian Cary 5E UV-Vis-NIR spectrometer. The spectra were recorded from 350 nm to 750 nm at room temperature. The ferrous $O_2$-ligated forms were measured, without additional treatment (as-purified), soon after protein purification, while the unligated form was obtained by adding 1% v/v sodium dithionite saturated solution to the sample, after $N_2$ bubbling.

*Resonance Raman spectroscopy*

The resonance Raman (RR) spectra were measured on a Dilor XY-800 Raman spectrometer in low-dispersion mode, associated to a liquid $N_2$-cooled CCD detector (slit width = 200 μm), with a $Kr^+$ laser operating at 413.1 nm as the excitation source (Spectra-Physics BeamLok 2060). The applied laser power was 10 mW (*Bpe*GReg proteins) and 15 mW (*Av*GReg variants). The samples had a final concentration of 40 μM, and were magnetically stirred at 500 rpm to avoid local heating and photochemical decomposition. Six spectra were recorded with 120-180 s integration time, depending on the protein sample. To remove spikes due to cosmic rays, the highest and lowest data points for each frequency value were removed and averaged over the remaining values with an in-house written program.

*Ligand binding kinetics and data analysis*

Laser flash photolysis experiments were performed to measure the CO and $O_2$ binding kinetics at 20 °C using a laser photolysis system (Edinburgh Instruments LP920, UK) equipped with a frequency-doubled, Q-switched Nd:YAG laser (Quanta-Ray, Spectra Physics). A laser flash of 532 nm was used.

The carbon monoxide (CO)–ferrous Hb complexes were prepared in sealed 4 × 10 mm quartz cuvettes with 1 ml of 100 mM potassium phosphate buffer (pH 7.0) containing 1 mM EDTA. The buffer was equilibrated with mixtures of CO and $N_2$ in different ratios to obtain CO concentrations of 50–800 μM by using a gas mixer (HighTech System;

Bronkhorst, The Netherlands). Saturated sodium dithionite solution (10 µl) was added and the protein was injected to a final concentration of ~4 µM. Formation of the CO–ferrous Hb complex was verified by UV/visible absorption spectroscopy. Recombination of the photo-dissociated CO ligand was monitored at 418 nm (*Bpe*GReg) or 421 nm (*Av*GReg).

$O_2$/CO competition studies were performed with the ferrous oxygenated (as-purified) form of the GCS. Sealed cuvettes containing 100 mM phosphate buffer pH 7.0 were flushed with $O_2$/CO mixtures ($O_2$ concentrations between 250 and 812.5 µM, and CO concentrations between 350 and 800 µM). The protein was added to the experimental cuvettes immediately prior to the photolysis experiment. The CO/$O_2$ displacement was followed at 418 nm and 436 nm for *Bpe*GReg and at 421 nm and 436 nm for *Av*GReg.

The data obtained were analyzed with MATLAB® (The MathWorks, Inc., Natick, Massachusetts, USA) and fitted with Origin (OriginLab, Northampton, Massachusetts, USA). The time courses for CO rebinding followed a mono exponential decay and were fitted to the minimum reaction mechanism (scheme 1) with equations as described elsewhere (42,64).

$$GCS + CO \underset{k_{CO}}{\overset{k'_{CO}}{\rightleftarrows}} GCS - CO \qquad \text{(Scheme 1)}$$

The $O_2$/CO competition time courses fitted with a two-exponential process (Scheme 2, (42)), valid also for the globin domain alone:

$$GCS - O_2 + CO \xrightarrow{k'_{CO}, k_{O2}} GCS - CO + O_2 \qquad \text{(Scheme 2a)}$$

$$GCS + O_2 \xrightarrow{k'_{O2}} GCS - O_2 \qquad \text{(Scheme 2b)}$$

The values of $k'_{O2}$, $k_{O2}$, and $k'_{CO}$ were obtained according to the equations:

$$k_f = k'_{O2}[O_2] + k'_{CO}[CO] + k_{O2} \qquad \text{(Equation 1)}$$



Antioxidants and Redox Signaling
Structural and functional characterization of the globin-coupled sensors of *Azotobacter vinelandii* and *Bordetella pertussis* (DOI: 10.1089/ars.2018.7690)
This paper has been peer-reviewed and accepted for publication, but has yet to undergo copyediting and proof correction. The final published version may differ from this proof.

$$k_s = \frac{k_{O2}}{1 + \frac{k'_{O2}[O_2]}{k'_{CO}[CO]}} \quad \text{(Equation 2)}$$

where $k_f$ is the fast observed reaction constant $k_{obs}$, and $k_s$ is the slow $k_{obs}$ at a given ligand concentration.

The slower $O_2$ dissociation rate constant was determined with a ligand replacement method using stopped flow, as already described (41). Experiments were performed at 20 °C in triplicates on an Applied Photophysics SX20 stopped-flow spectrometer apparatus equipped with the Pro-Data™ software suite. After measurements, the raw data were further analyzed with Origin (OriginLab, Northampton, Massachusetts, USA). The oxygenated protein solution was rapidly mixed with an $O_2$/CO mixture (the final protein concentration after mixing was 2.5 µM) in 100 µM potassium phosphate buffer pH 7.5, 1 mM EDTA.

*Diguanylate cyclase assay*

A HPLC-based DGC assay was adapted from (54) and performed in triplicate to quantify c-di-GMP synthesis by *Av*GReg. Shortly, 10 µM of enzyme was incubated at 37 °C with 20 to 65 µM GTP in 50 mM TRIS-HCl pH 7.5, 50 mM NaCl and 10 mM $MgCl_2$. Aliquots were taken at different times and the reaction was rapidly stopped with one-fourth volume of 0.5 M EDTA pH 8.0, which ensures repeatability in the measurement of more time points in a few seconds time frame, as required for initial rate determination of enzymatic processes. For deproteination, the stopped reaction mixture was heated for 5 min at 95 °C and centrifuged for 10 minutes at 11,300 x g. 20 µl of the supernatant was injected onto an Adsorbosphere Nucleotide-Nucleoside RP C18 HPLC column (Alltech, 250x4.6 mm) equipped with the same type guard column (Alltech/Grade, 7.5x4.6 mm). As mobile phase, 0.15 M $NaH_2PO_4$ and 40% acetonitrile was used. A relatively rapid linear gradient from 0% to 35% acetonitrile, for 10 minutes at 1 ml $min^{-1}$, was applied to separate GTP, c-di-GMP and pGpG, with which we could efficiently process the high number of samples produced. Known amounts of all three molecules were used for standardization.

Given the high sensitivity of *Av*GReg to product inhibition, low substrate concentrations were used. When the substrate concentration [S] << $K_m$, then [S] is almost negligible and the Michaelis-Menten's equation becomes:



Antioxidants and Redox Signaling
Structural and functional characterization of the globin-coupled sensors of *Azotobacter vinelandii* and *Bordetella pertussis* (DOI: 10.1089/ars.2018.7690)
This paper has been peer-reviewed and accepted for publication, but has yet to undergo copyediting and proof correction. The final published version may differ from this proof.

$$v_i = \frac{V_{max}[S]}{K_m}$$

Given that $V_{max} = k_{cat}[E]_0$, in our experimental conditions the enzyme specificity constant ($k_{cat}/K_m$) can be calculated from Michaelis-Menten plots.

*Crystallization, structure determination, and refinement*

Crystallization of *Av*GReg-Gb and *Bpe*GReg-Gb* was achieved using the sitting drop vapour diffusion method. *Av*GReg-Gb crystals were obtained by equilibrating at 4 °C the protein solution (30 mg $ml^{-1}$) against 33% PEG 6000 and 10 mM Na-citrate. The crystals diffracted up to 2.83 Å resolution, using synchrotron radiation (Elettra - Sincrotrone Trieste S.C.p.A, Trieste, Italy; XRD1 beamline). They belong to the monoclinic $P2_1$ space group and two *Av*GReg-Gb molecules per asymmetric unit (estimated solvent content 33%) (Table 4). *Bpe*GReg-Gb* crystals grew at 4 °C by using two different ionic and pH conditions: 1.6 M magnesium sulphate and 0.1 M MES pH 6.5 (condition 1: *Bpe*GReg-Gb*) or 0.8 - 1 M ammonium sulphate and 0.1 M TRIS-HCl pH 6.0 - 9.0 (condition 2: *Bpe*GReg-Gb*-2). The crystals grown under condition 1 and 2 diffracted up to 3.20 Å and 1.55 Å resolution, respectively, using synchrotron radiation (at SOLEIL and ESRF facilities, France). Both crystal forms belong to the *C*2 space group, but with different cell parameters, and contain two protein molecules in the asymmetric unit (estimated solvent content 48.25 % for *Bpe*GReg-Gb*, and 34.69 % for *Bpe*GReg-Gb*-2) (Table 4). MOSFLM (31), SCALA (18), and the CCP4 suite programs (71) were used for reducing, scaling and analysing all the collected data.

The *Bpe*GReg-Gb*-2 structure was solved with a combination of single wavelength anomalous dispersion (based on the heme-Fe atom anomalous signal) and molecular replacement. Few regions of the structure were built based on the SAD data. This partial model was used to determine the remaining phases with Phaser molecular replacement program (35). The molecular model was checked manually with COOT (17) and refined with REFMAC5 (37,38) to the maximum resolution (Table 4). The *Bpe*GReg-Gb*-2 refined structure was used as starting model (as a monomer) to solve the *Bpe*GReg-Gb* and the *Av*GReg-Gb dimeric structures with Phaser (35). The resulting structures were remodeled by using COOT (17) and refined with REFMAC5 (37,38) (Table 4). Their stereo chemical quality was assessed with MolProbity (9) and the quaternary assemblies were identified



Antioxidants and Redox Signaling
Structural and functional characterization of the globin-coupled sensors of *Azotobacter vinelandii* and *Bordetella pertussis* (DOI: 10.1089/ars.2018.7690)
This paper has been peer-reviewed and accepted for publication, but has yet to undergo copyediting and proof correction. The final published version may differ from this proof.

with PISA (30). Finally, the atomic coordinates and the structure factors have been deposited in the Protein Data Bank (www.rcsb.org) with entry codes 4UII (*Av*GReg-Gb), 6I2Z (*Bpe*GReg-Gb*), and 4UIQ (*Bpe*GReg-Gb*-2).

**Acknowledgements**

This work was supported by the Fund of Scientific Research – Flanders (FWO) grant no. G.0247.09N and supported by the University of Antwerp through the GOA biofilm project 25624 (GOA BOF UA 2011-2014) and the GOA-BOF project 28312. F.G. is a PhD fellow of the Fund of Scientific Research – Flanders (FWO). A.D.S. was funded by a PhD grant of the Innovation by Science and Technology (121339) (IWT, Belgium). The authors thank Miroslaw Tarnawski and Thomas Barends for making the *Ec*DosC model (full-length) available. The authors have no conflict of interest to declare.



Antioxidants and Redox Signaling
Structural and functional characterization of the globin-coupled sensors of *Azotobacter vinelandii* and *Bordetella pertussis* (DOI: 10.1089/ars.2018.7690)
This paper has been peer-reviewed and accepted for publication, but has yet to undergo copyediting and proof correction. The final published version may differ from this proof.

**Abbreviations**:

*Af*GcHK = globin-coupled histidine kinase from *Anaeromyxobacter sp.* Fw109-5

*Av*GReg = globin-coupled regulator from *Azotobacter vinelandii*

*Av*GReg-Gb = *Av*GReg globin domain

*Av*GRegYB10F = *Av*GReg with Tyr(44) mutated to Phe

*Av*GReg178 = recombinant and reconstructed (heme + apoprotein) globin domain

*Bj*FixL = *Bradyrhizobium japonicum* nitrogen fixation gene expression regulator

*Bs*HemAT = *Bacillus subtilis* heme-based aerotaxis transducer

*Bpe*GReg = globin-coupled sensor from *Bordetella pertussis*

*Bpe*GReg* = *Bpe*GReg with cysteines (Cys16, 45, 114, 154) mutated to serines

*Bpe*GReg-Gb = *Bpe*GReg globin domain

*Bpe*GReg-Gb* = *Bpe*GRegGb with cysteines (Cys16, 45, 114, 154) mutated to serines

c-di-GMP, cyclic-di-(3',5')-GMP

DGC = diguanylate cyclase

*Ec*DosC = *E. coli* globin-coupled sensor with DGC activity

*Ec*DosC-heme = isolated globin domain of the *E. coli* globin-coupled sensor

GCS = globin-coupled sensor

*Gs*GCS$^{162}$ = sensor domain from the *Geobacter sulfurreducens* globin-coupled sensor

PDE = phosphodiesterase

*Rm*FixL* = soluble truncated domain of the *Rhizobium meliloti* nitrogen fixation gene expression regulator

Rmsd = root mean squared deviation

RR, Resonance Raman spectroscopy

*Rr*CooA = *Rhodospirillum rubrum* carbon monoxide oxidation activator; sGC, soluble guanylyl cyclase

*Sw*Mb = sperm whale myoglobin



Antioxidants and Redox Signaling
Structural and functional characterization of the globin-coupled sensors of *Azotobacter vinelandii* and *Bordetella pertussis* (DOI: 10.1089/ars.2018.7690)
This paper has been peer-reviewed and accepted for publication, but has yet to undergo copyediting and proof correction. The final published version may differ from this proof.

**REFERENCES**

1. Antonini, E. and Brunori M. Hemoglobin and myoglobin in their reactions with ligands. 1971: North-Holland Pub. Co.
2. Aono S, Kato T, Matsuki M, Nakajima H, Ohta T, Uchida T, and Kitagawa T. Resonance Raman and ligand binding studies of the oxygen-sensing signal transducer protein HemAT from *Bacillus subtilis*. *J Biol Chem* 277: 13528-13538, 2002.
3. Bart MJ, van Gent M, van der Heide HG, Boekhorst J, Hermans P, Parkhill J, and Mooi FR. Comparative genomics of prevaccination and modern *Bordetella pertussis* strains. *BMC Genomics* 11: 627, 2010.
4. Bart MJ, Zeddeman A, van der Heide HG, Heuvelman K, van Gent M, and Mooi FR. Complete genome sequences of *Bordetella pertussis* isolates B1917 and B1920, representing two predominant global lineages. *Genome Announc* 2: pii: e01301-14, 2014.
5. Brunori M and Schuster TM. Kinetic studies of ligand binding to hemoglobin and its isolated subunits by the temperature jump relaxation method. *J Biol Chem* 244: 4046-4053, 1969.
6. Burns JL, Deer DD, and Weinert EE. Oligomeric state affects oxygen dissociation and diguanylate cyclase activity of globin coupled sensors. *Mol Biosyst* 10: 2823-2826, 2014.
7. Burns JL, Rivera S, Deer DD, Joynt SC, Dvorak D, and Weinert EE. Oxygen and bis(3',5')-cyclic dimeric guanosine monophosphate binding control oligomerization state equilibria of diguanylate cyclase-containing globin coupled sensors. *Biochemistry* 55: 6642-6651, 2016.
8. Centeno JA. Evidence of dithionite contribution to the low-frequency resonance Raman spectrum of reduced and mixed-valence cytochrome c oxidase. *Arch Biochem Biophys*. 292: 624-628, 1992.
9. Chen VB, Arendall WB, III, Headd JJ, Keedy DA, Immormino RM, Kapral GJ, Murray LW, Richardson JS, and Richardson DC. MolProbity: all-atom structure validation for macromolecular crystallography. *Acta Crystallogr D Biol Crystallogr* 66: 12-21, 2010.

10. Conover MS, Sloan GP, Love CF, Sukumar N, and Deora R. The Bps polysaccharide of *Bordetella pertussis* promotes colonization and biofilm formation in the nose by functioning as an adhesin. *Mol Microbiol* 77: 1439-1455, 2010.
11. Das TK, Couture M, Ouellet Y, Guertin M, and Rousseau DL. Simultaneous observation of the O---O and Fe---$O_2$ stretching modes in oxyhemoglobins. *Proc Natl Acad Sci* USA 98: 479-484, 2001.
12. Das TK, Friedman JM, Kloek AP, Goldberg DE, and Rousseau DL. Origin of the anomalous Fe-CO stretching mode in the CO complex of *Ascaris* hemoglobin. *Biochemistry* 39: 837-842, 2000.
13. Deinum G, Stone JR, Babcock GT, Marletta MA. Binding of nitric oxide and carbon monoxide to soluble guanylate cyclase as observed with Resonance raman spectroscopy. *Biochemistry* 35: 1540-1547, 1996.
14. Dewilde S, Mees K, Kiger L, Lechauve C, Marden MC, Pesce A, Bolognesi M, and Moens L. Expression, purification, and crystallization of neuro- and cytoglobin. *Methods Enzymol* 436: 341-357, 2008.
15. Dewilde S, Kiger L, Burmester T, Hankeln T, Baudin-Creuza V, Aerts T, Marden MC, Caubergs R, and Moens L. Biochemical characterization and ligand binding properties of neuroglobin, a novel member of the globin family. *J Biol Chem* 276: 38949-38955, 2001.
16. Dufour D, Leung V, and Lévesque CM. Bacterial biofilm: structure, function and antimicrobial resistence. *Endod Top* 22: 2-16, 2012.
17. Emsley P, Lohkamp B, Scott WG, and Cowtan K. Features and development of Coot. *Acta Crystallogr D Biol Crystallogr* 66: 486-501, 2010.
18. Evans P. Scaling and assessment of data quality. *Acta Crystallogr D Biol Crystallogr* 62: 72-82, 2006.
19. Freitas TA, Hou S, and Alam M. The diversity of globin-coupled sensors. *FEBS Lett* 552: 99-104, 2003.
20. Germani F, Moens L, and Dewilde S. Haem-based sensors: a still growing old superfamily. *Adv Microb Physiol* 63: 1-47, 2013.
21. Gibson QH, Olson JS, McKinnie RE, and Rohlfs RJ. A kinetic description of ligand binding to sperm whale myoglobin. *J Biol Chem* 261: 10228-10239, 1986.

22. Gilles-Gonzalez MA, Gonzalez G, Perutz MF, Kiger L, Marden MC, and Poyart C. Heme-based sensors, exemplified by the kinase FixL, are a new class of heme protein with distinctive ligand binding and autoxidation. *Biochemistry* 33: 8067-8073, 1994.
23. Guttenplan SB and Kearns DB. Regulation of flagellar motility during biofilm formation. *FEMS Microbiol Rev* 37: 849-871, 2013.
24. Hirota S, Ogura T, Appelman E.H., Shinzawaitoh K, Yoshikawa S, and Kitagawa T. Observation of a new oxygen-isotope-sensitive Raman band for oxyhemoproteins and its implication in heme pocket structures. *J Am Chem Soc* 116: 10564-10570, 1994.
25. Hu SZ, Smith K, and Spiro TG. Assignment of protoheme resonance raman spectrum by heme labeling in myoglobin. *J Am Chem Soc* 118: 12638-12646, 1996.
26. Jenal U, Reinders A and Lori C. Cyclic di-GMP: second messenger extraordinaire. *Nat Rev Microbiol* 15:271-284, 2017.
27. Kerr EA, Yu NT, Bartnicki DE, and Mizukami H. Resonance Raman studies of CO and $O_2$ binding to elephant myoglobin (distal His(E7)----Gln). *J Biol Chem* 260: 8360-8365, 1985.
28. Kitanishi K, Kobayashi K, Kawamura Y, Ishigami I, Ogura T, Nakajima K, Igarashi J, Tanaka A, and Shimizu T. Important roles of Tyr43 at the putative heme distal side in the oxygen recognition and stability of the Fe(II)-$O_2$ complex of YddV, a globin-coupled heme-based oxygen sensor diguanylate cyclase. *Biochemistry* 49: 10381-10393, 2010.
29. Kitanishi K, Kobayashi K, Uchida T, Ishimori K, Igarashi J, and Shimizu T. Identification and functional and spectral characterization of a globin-coupled histidine kinase from *Anaeromyxobacte*r sp. Fw109-5. *J Biol Chem* 286: 35522-35534, 2011.
30. Krissinel E, and Henrick K. Inference of macromolecular assemblies from crystalline state. *J Mol Biol* 372: 774-797, 2007.
31. Leslie AG. The integration of macromolecular diffraction data. *Acta Crystallogr D Biol Crystallogr* 62: 48-57, 2006.
32. Martinez LC and Vadyvaloo V. Mechanisms of post-transcriptional gene regulation in bacterial biofilms. *Front Cell Infect Microbiol* 4: 38, 2014.
33. Martinkova M, Kitanishi K, and Shimizu T. Heme-based globin-coupled oxygen sensors: linking oxygen binding to functional regulation of diguanylate cyclase, histidine kinase, and methyl-accepting chemotaxis. *J Biol Chem* 288: 27702-27711, 2013.

34. Maunders E and Welch M. Matrix exopolysaccharides; the sticky side of biofilm formation. *FEMS Microbiol Lett* 363:fnx120, 2017.

35. McCoy AJ, Grosse-Kunstleve RW, Adams PD, Winn MD, Storoni LC, and Read RJ. Phaser crystallographic software. *J Appl Crystallogr* 40: 658-674, 2007.

36. Mishra M, Parise G, Jackson KD, Wozniak DJ, and Deora R. The BvgAS signal transduction system regulates biofilm development in *Bordetella*. *J Bacteriol* 187: 1474-1484, 2005.

37. Murshudov GN, Vagin AA, and Dodson EJ. Refinement of macromolecular structures by the maximum-likelihood method. *Acta Crystallogr D Biol Crystallogr* 53: 240-255, 1997.

38. Murshudov GN, Vagin AA, Lebedev A, Wilson KS, and Dodson EJ. Efficient anisotropic refinement of macromolecular structures using FFT. *Acta Crystallogr D Biol Crystallogr* 55: 247-255, 1999.

39. Nagai K, Kitagawa T, and Morimoto H. Quaternary structures and low frequency molecular vibrations of haems of deoxy and oxyhaemoglobin studied by resonance raman scattering. *J Mol Biol* 136: 271-289, 1980.

40. Nardini M, Pesce A, Thijs L, Saito JA, Dewilde S, Alam M, Ascenzi P, Coletta M, Ciaccio C, Moens L, and Bolognesi M. Archaeal protoglobin structure indicates new ligand diffusion paths and modulation of haem-reactivity. *EMBO Rep* 9: 157-163, 2008.

41. Olson JS. Stopped-flow, rapid mixing measurements of ligand binding to hemoglobin and red cells. *Methods Enzymol* 76: 631-651, 1981.

42. Olson JS, Foley EW, Maillet DH, Paster EV, Measurement of Rate Constants for Reactions of $O_2$, CO and NO with Hemoglobin. In: Nagel RL (eds) Hemoglobin Disorders, Methods in Molecular Biology, Humana Press Inc., Totowa NJ, 82, 65- 91, 2003.

43. Othman S, Richaud P, Vermeglio A, and Desbois A. Evidence for a proximal histidine interaction in the structure of cytochromes c in solution: a resonance Raman study. *Biochemistry* 35: 9224-9234, 1996.

44. Pesce A, Thijs L, Nardini M, Desmet F, Sisinni L, Gourlay L, Bolli A, Coletta M, Van DS, Wan X, Alam M, Ascenzi P, Moens L, Bolognesi M, and Dewilde S. HisE11 and HisF8 provide bis-histidyl heme hexa-coordination in the globin domain of *Geobacter sulfurreducens* globin-coupled sensor. *J Mol Biol* 386: 246-260, 2009.

45. Pesce A, Tilleman L, Dewilde S, Ascenzi P, Coletta M, Ciaccio C, Bruno S, Moens L, Bolognesi M, and Nardini M. Structural heterogeneity and ligand gating in ferric *Methanosarcina acetivorans* protoglobin mutants. *IUBMB. Life* 63: 287-294, 2011.
46. Pesce A, Tilleman L, Donne J, Aste E, Ascenzi P, Ciaccio C, Coletta M, Moens L, Viappiani C, Dewilde S, Bolognesi M, and Nardini M. Structure and haem-distal site plasticity in *Methanosarcina acetivorans* protoglobin. *PLoS ONE* 8: e66144, 2013.
47. Pesce A, Nardini M, Dewilde S, Ascenzi P, Burmester T, Hankeln T, Moens L, and Bolognesi M. Human neuroglobin: crystals and preliminary X-ray diffraction analysis. *Acta Crystallogr D Biol Crystallogr* 58: 1848-1850, 2002.
48. Poole RK and Hill S. Respiratory protection of nitrogenase activity in *Azotobacter vinelandii*--roles of the terminal oxidases. *Biosci Rep* 17: 303-317, 1997.
49. Purcell EB and Tamayo R. Cyclic diguanylate signaling in Gram-positive bacteria. *FEMS Microbiol Rev* 40: 753-773, 2016.
50. Rivera S, Burns JL, Vansuch GE, Chica B, and Weinert EE. Globin domain interactions control heme pocket conformation and oligomerization of globin coupled sensors. *J Inorg Biochem* 164: 70-76, 2016.
51. Rivera S, Young PG, Hoffer ED, Vansuch GE, Metzler CL, Dunham CM, and Weinert EE. Structural insights into oxygen-dependent signal transduction within globin coupled sensors. Inorg. Chem. 57: 14386-14395, 2018.
52. Römling U and Galperin MY. Discovery of the second messenger Cyclic di-GMP. *Methods Mol Biol* 1657:1-8, 2017.
53. Ryan RP. Cyclic di-GMP signalling and the regulation of bacterial virulence. *Microbiology* 159: 1286-1297, 2013.
54. Ryjenkov DA, Tarutina M, Moskvin OV, and Gomelsky M. Cyclic diguanylate is a ubiquitous signaling molecule in bacteria: insights into biochemistry of the GGDEF protein domain. *J Bacteriol* 187: 1792-1798, 2005.
55. Setubal JC, Dos SP, Goldman BS, Ertesvag H, Espin G, Rubio LM, Valla S, Almeida NF, Balasubramanian D, Cromes L, Curatti L, Du Z, Godsy E, Goodner B, Hellner-Burris K, Hernandez JA, Houmiel K, Imperial J, Kennedy C, Larson TJ, Latreille P, Ligon LS, Lu J, Maerk M, Miller NM, Norton S, O'Carroll IP, Paulsen I, Raulfs EC, Roemer R, Rosser J, Segura D, Slater S, Stricklin SL, Studholme DJ, Sun J, Viana CJ, Wallin E, Wang B,

Wheeler C, Zhu H, Dean DR, Dixon R, and Wood D. Genome sequence of *Azotobacter vinelandii*, an obligate aerobe specialized to support diverse anaerobic metabolic processes. *J Bacteriol* 191: 4534-4545, 2009.

56. Shimizu T, Huang D, Yan F, Stranava M, Bartosova M, Fojtikova V, and Martinkova M. Gaseous $O_2$, NO, and CO in signal transduction: structure and function relationships of heme-based gas sensors and heme-redox sensors. *Chem Rev* 115: 6491-6533, 2015.
57. Sondermann H, Shikuma NJ, and Yildiz FH. You've come a long way: c-di-GMP signaling. *Curr Opin Microbiol* 15: 140-146, 2012.
58. Song S, Boffi A, Chiancone E, and Rousseau DL. Protein-heme interactions in hemoglobin from the mollusc *Scapharca inaequivalvis*: evidence from resonance Raman scattering. *Biochemistry* 32: 6330-6336, 1993.
59. Spiro TG and Li XY. Resonance Raman spectroscopy of metalloporphyrins. *Biological applications of Raman spectroscopy* 3: 1-37, 1988.
60. Takahashi S, Ishikawa, Takeuchi N, Ikeda-Saito M, Yoshida Y, and Rousseau DL. Oxygen-bound heme-heme oxygenase complex: evidence for a highly bent structure of the coordinated oxygen. *J Am Chem Soc* 117: 6002-6006, 1995.
61. Takahashi S, Wang J, Rousseau DL, Ishikawa K, Yoshida T, Takeuchi N, and Ikeda-Saito M. Heme-heme oxygenase complex: structure and properties of the catalytic site from resonance Raman scattering. *Biochemistry* 33: 5531-5538, 1994.
62. Tamura K, Tanaka Y, Oue S, Tsukamoto K, Nomura M, Tsuchiya T, Adachi S, Takahashi S, Iizuka T, and Shiro Y. Nature of endogenous ligand binding to heme iron in oxygen sensor FixL. *J Am Chem Soc* 118: 9434-9435, 1996.
63. Tarnawski M, Barends TR, and Schlichting I. Structural analysis of an oxygen-regulated diguanylate cyclase. *Acta Crystallogr D Biol Crystallogr* 71: 2158-2177, 2015.
64. Thijs L, Vinck E, Bolli A, Trandafir F, Wan X, Hoogewijs D, Coletta M, Fago A, Weber RE, Van Doorslaer S, Ascenzi P, Alam M, Moens L, and Dewilde S. Characterization of a globin-coupled oxygen sensor with a gene-regulating function. *J Biol Chem* 282: 37325-37340, 2007.
65. Tomita T, Ogura T, Tsuyama S, Imai Y, and Kitagawa T. Effects of GTP on bound nitric oxide of soluble guanylate cyclase probed by resonance Raman spectroscopy. *Biochemistry* 36: 10155-10160, 1997.



Antioxidants and Redox Signaling
Structural and functional characterization of the globin-coupled sensors of *Azotobacter vinelandii* and *Bordetella pertussis* (DOI: 10.1089/ars.2018.7690)
This paper has been peer-reviewed and accepted for publication, but has yet to undergo copyediting and proof correction. The final published version may differ from this proof.

66. Tsai AL, Berka V, Martin E and Olson JS. A "Sliding Scale Rule" for Selectivity among NO, CO and $O_2$ by Heme Protein Sensors. *Biochemistry* 51:172-186, 2012.

67. Uchida T, Ishikawa H, Takahashi S, Ishimori K, Morishima I, Ohkubo K, Nakajima H, and Aono S. Heme environmental structure of CooA is modulated by the target DNA binding. Evidence from resonance Raman spectroscopy and CO rebinding kinetics. *J Biol Chem* 273: 19988-19992, 1998.

68. Uchida T and Kitagawa T. Mechanism for transduction of the ligand-binding signal in heme-based gas sensory proteins revealed by resonance Raman spectroscopy. *Acc Chem Res* 38: 662-670, 2005.

69. Vinogradov SN and Moens L. Diversity of globin function: enzymatic, transport, storage, and sensing. *J Biol Chem* 283: 8773-8777, 2008.

70. Wan X, Tuckerman JR, Saito JA, Freitas TA, Newhouse JS, Denery JR, Galperin MY, Gonzalez G, Gilles-Gonzalez MA, and Alam M. Globins synthesize the second messenger bis-(3'-5')-cyclic diguanosine monophosphate in bacteria. *J Mol Biol* 388: 262-270, 2009.

71. Winn MD, Ballard CC, Cowtan KD, Dodson EJ, Emsley P, Evans PR, Keegan RM, Krissinel EB, Leslie AG, McCoy A, McNicholas SJ, Murshudov GN, Pannu NS, Potterton EA, Powell HR, Read RJ, Vagin A, and Wilson KS. Overview of the CCP4 suite and current developments. *Acta Crystallogr D Biol Crystallogr* 67: 235-242, 2011.

72. Yang, J., et al., The I-TASSER Suite: protein structure and function prediction. *Nat Methods* 12: 7-8, 2015.

73. Yeh SH. Pertussis: persistent pathogen, imperfect vaccines. *Expert Rev Vaccines* 2: 113-127, 2003.

74. Yeh SR, Couture M, Ouellet Y, Guertin M, and Rousseau DL. A cooperative oxygen binding hemoglobin from *Mycobacterium tuberculosis*. Stabilization of heme ligands by a distal tyrosine residue. *J Biol Chem* 275: 1679-1684, 2000.

75. Zhang W and Phillips GN, Jr. Structure of the oxygen sensor in *Bacillus subtilis*: signal transduction of chemotaxis by control of symmetry. *Structure* 11: 1097-1110, 2003.



Antioxidants and Redox Signaling
Structural and functional characterization of the globin-coupled sensors of *Azotobacter vinelandii* and *Bordetella pertussis* (DOI: 10.1089/ars.2018.7690)
This paper has been peer-reviewed and accepted for publication, but has yet to undergo copyediting and proof correction. The final published version may differ from this proof.

**Table 1. UV/VIS maxima of the different forms of *Av*GReg and *Bpe*GReg**

| ***Av*GReg** (wavelength in nm) | | | | | | |
|---|---|---|---|---|---|---|
| As purified ($Fe^{2+}$-$O_2$) | 413 | | | 541 | | 580 |
| Reduced ($Fe^{2+}$) | | | 434 | | 560 | |
| CO-ligated | | 421 | | 542 | 568 | |
| ***Bpe*GReg** (wavelength in nm) | | | | | | |
| As purified ($Fe^{2+}$-$O_2$) | 415 | | | 547 | | 582 |
| Reduced ($Fe^{2+}$) | | | 432 | | 561 | |
| CO-ligated | | 422 | | 544 | 570 | |



Antioxidants and Redox Signaling
Structural and functional characterization of the globin-coupled sensors of *Azotobacter vinelandii* and *Bordetella pertussis* (DOI: 10.1089/ars.2018.7690)
This paper has been peer-reviewed and accepted for publication, but has yet to undergo copyediting and proof correction. The final published version may differ from this proof.

**Table 2. Resonance Raman vibrational modes values of different hemoproteins**

| Hemoprotein | Vibrational modes ($cm^{-1}$) | | | | | Ref |
|---|---|---|---|---|---|---|
| | $\nu_4$ | $\nu_3$ | $\nu_2$ | $\nu_{Fe-His}$ | $\nu_{Fe-O2}$ | |
| $O_2$-*Av*GReg | 1379 | 1505 | 1583 | - | 563/573 | This study |
| *Av*GReg(FeII) | 1357 | 1474 | 1567 | 227 | - | |
| $O_2$-*Av*GReg-Gb | 1376 | 1505 | 1579 | - | 561/573 | |
| *Av*GReg-Gb(FeII) | 1356 | 1471 | 1563 | 214(b) | - | |
| $O_2$-*Bpe*GReg | 1373 | 1501 | n.d. | - | n.d. | This study |
| *Bpe*GReg (FeII) | 1357 | 1472 | 1565 | 229 | - | |
| $O_2$-*Bpe*GReg-Gb | 1380 | 1507 | 1583 | - | 563 | |
| *Bpe*GReg-Gb (FeII) | 1359 | 1474 | 1567 | 233 | - | |
| $O_2$-*Bpe*GReg* | 1373 | 1502 | 1577 | - | 556 | This study |
| *Bpe*GReg* (FeII) | 1356 | 1472 | 1564 | 229 | - | |
| $O_2$-*Bpe*GReg-Gb* | 1375 | 1502 | 1578 | - | 560 | |
| *Bpe*GReg-Gb* (FeII) | 1356 | 1472 | 1564 | 230(b) | - | |
| $O_2$-*Sw*Mb | 1377 | 1507 | 1584 | - | 569 | (60,61) |
| *Sw*Mb(FeII) | 1356 | 1473 | 1564 | 220 | - | |
| †*Av*GReg(FeIII) | 1375 | 1506 | 1588 | - | - | (64) |
| †*Av*GReg(FeII) | 1361 | 1470 | 1592 | n.d. | - | |
| †$O_2$-*Av*GReg178 | 1372 | 1502 | 1575 | - | n.d. | |
| †*Av*GReg178(FeII) | 1354 | 1470 | 1562 | 220 | - | |
| $O_2$-*Bs*HemAT | 1372 | 1501 | 1578 | - | 560 | (2) |
| *Bs*HemAT(FeII) | 1352 | 1469 | 1558 | 225 | - | |
| $O_2$-*Ec*DosC-heme | 1377 | 1499 | 1581 | - | 565 | (28) |
| *Ec*DosC-heme(FeII) | 1353 | 1470 | 1564 | 227 | - | |
| $O_2$-*Af*GcHK | 1375 | 1501 | 1579 | - | 557 | (29) |
| *Af*GcHK(FeII) | 1354 | 1470 | 1558 | 223 | - | |
| $O_2$-*Rm*FixL* | 1376 | 1502 | 1577 | - | n.d. | (62) |
| *Rm*FixL*(FeII) | 1355 | 1470 | 1558 | 212 | - | |



Antioxidants and Redox Signaling
Structural and functional characterization of the globin-coupled sensors of *Azotobacter vinelandii* and *Bordetella pertussis* (DOI: 10.1089/ars.2018.7690)
This paper has been peer-reviewed and accepted for publication, but has yet to undergo copyediting and proof correction. The final published version may differ from this proof.

| | | | | | | |
|---|---|---|---|---|---|---|
| *Rr*CooA(FeII) | 1359 | 1491 | 1579 | n.d. | - | (67,68) |
| sGC(FeII) | 1358 | 1471 | 1562 | 204 | - | (13,65) |

Error is 2 $cm^{-1}$, b=broad peak, n.d.=not detected

*Av*GReg and *Av*GReg-Gb: *in vivo* folded *A. vinelandii* full-length and truncated globin-coupled regulator; *Bpe*GReg and *Bpe*GReg*: globin-coupled sensor from *Bordetella pertussis* wild-type and with mutated cysteines (Cys16, 45, 114, 154); *Bpe*GReg-Gb and *Bpe*GReg-Gb*: isolated globin domain of *Bpe*GReg and *Bpe*GReg*: *Sw*Mb: *Sperm whale* myoglobin; $^{\dagger}$*Av*GReg and $^{\dagger}$*Av*GReg178: *in vitro* refolded *A. vinelandii* full-length and truncated globin-coupled regulator; *Bs*HemAT: heme-based aerotaxis transducer from *Bacillus subtilis*; *Ec*DosC-heme: isolated heme-binding domain from *Ec*DosC, a globin-coupled sensor with DGC activity from *E. coli*; *Af*GcHK: globin-coupled histidine kinase from *Anaeromyxobacter sp.* Fw109-5; *Rm*FixL*: soluble truncated domain of the *Rhizobium meliloti* nitrogen fixation gene expression regulator; *Rr*CooA: *Rhodospirillum rubrum* carbon monoxide oxidation activator; sGC: soluble guanylyl cyclase.



Antioxidants and Redox Signaling
Structural and functional characterization of the globin-coupled sensors of *Azotobacter vinelandii* and *Bordetella pertussis* (DOI: 10.1089/ars.2018.7690)
This paper has been peer-reviewed and accepted for publication, but has yet to undergo copyediting and proof correction. The final published version may differ from this proof.

**Table 3. Kinetics and equilibrium constants for ligand binding to some hemoproteins**

| Hemoprotein | CO | $O_2$ | | | Ref |
|---|---|---|---|---|---|
| | $k'_{CO}$ ($10^6$ $M^{-1}$ $s^{-1}$) | $k'_{O2}$ ($10^6$ $M^{-1}$ $s^{-1}$) | $k_{O2}$ ($s^{-1}$) | $K_d = \frac{k_{off}}{k_{on}}$ ($10^{-6}$ M) | |
| *Av*GReg | 0.48±0.01 | 12.2±1.5 | 1732±377<br>0.53±0.05 | 141<br>0.04 | This study |
| *Av*GReg-Gb | 0.20±0.01 | - | - | - | This study |
| *Av*GRegYB10F | 0.31±0.01 | 20.2±1.3 | 18389±556<br>166±18 | 910<br>8.22 | This study |
| *Bpe*GReg | 0.60±0.01<br>0.01±0.01 | 24.02±1.5 | 4.0±0.1 | 0.17 | This study |
| *Bpe*GReg-Gb | 0.11±0.01 | - | - | - | This study |
| †*Av*GReg | 1 | -<br>- | 10.6<br>0.73 | -<br>- | (64) |
| †*Av*GReg178 | 1 | 424<br>5.2 | 10.6<br>0.13 | 0.025<br>0.025 | (64) |
| *Gs*GCS[162] | 6.80 | - | 23 | - | (44) |
| *Bs*HemAT | 0.34 | 19 | 1900<br>87 | 100<br>4.6 | (75) |
| *Bpe*GReg | 1.03<br>0.12 | 7.0 | 4.5 | 0.64 | (70) |
| *Ec*DosC | 0.22 | 0.9 | 13 | 14 | (28) |
| *Ec*DosC-heme | 0.40 | 1.4 | 22 | 16 | (28) |
| *Af*GcHK | 0.05 | 1.3<br>0.15 | 0.10 | 0.08<br>0.67 | (29) |



Antioxidants and Redox Signaling
Structural and functional characterization of the globin-coupled sensors of *Azotobacter vinelandii* and *Bordetella pertussis* (DOI: 10.1089/ars.2018.7690)
This paper has been peer-reviewed and accepted for publication, but has yet to undergo copyediting and proof correction. The final published version may differ from this proof.

| | | | | | |
|---|---|---|---|---|---|
| *Bj*FixL | - | 0.14 | 20 | 140 | (22) |
| *Sw*Mb | 0.50 | 14 | 11 | 1.27 | (5, 21) |

*Av*GReg and *Av*GReg-Gb: *in vivo* folded *A. vinelandii* full-length and truncated globin-coupled regulator; *Av*GRegYB10F: mutant of the two proteins in which the Tyr(44) at position B10 is replaced by Phe; *Bpe*GReg and *Bpe*GReg-Gb: full-length and truncated globin-coupled sensor from *Bordetella pertussis*; $^{\dagger}$*Av*GReg and $^{\dagger}$*Av*GReg178: *in vitro* refolded *A. vinelandii* full-length and truncated globin-coupled regulator; *Gs*GCS$^{162}$: sensor domain from the *Geobacter sulfurreducens* globin-coupled sensor; *Bs*HemAT: heme-based aerotaxis transducer from *Bacillus subtilis*; *Ec*DosC: globin-coupled sensor with DGC activity from *E. coli*; *Ec*DosC-heme: *Ec*DosC-isolated heme-binding domain; *Af*GcHK: globin-coupled histidine kinase from *Anaeromyxobacter sp.* Fw109-5; *Bj*FixL: *Bradyrhizobium japonicum* nitrogen fixation gene expression regulator; *Sw*Mb: *Sperm whale* myoglobin.



Antioxidants and Redox Signaling
Structural and functional characterization of the globin-coupled sensors of *Azotobacter vinelandii* and *Bordetella pertussis* (DOI: 10.1089/ars.2018.7690)
This paper has been peer-reviewed and accepted for publication, but has yet to undergo copyediting and proof correction. The final published version may differ from this proof.

**Table 4. Data collection and refinement statistics**

| **Data collection:** | ***Av*GReg-Gb** | ***Bpe*GReg-Gb*** | ***Bpe*GReg-Gb*-2** |
|---|---|---|---|
| Space group | $P2_1$ | $C2$ | $C2$ |
| Cell dimensions: | | | |
| *a*, *b*, *c* (Å) | 47.9, 49.5, 62.8 | 105.0, 86.7, 41.8 | 70.0, 53.1, 81.2 |
| *α*, *β*, *γ* (°) | 90.0, 91.8, 90.0 | 90.0, 93.3, 90.0 | 90.0, 93.2, 90.0 |
| Resolution (Å) | 30.5 - 2.83 | 52.4-3.20 | 42.3-1.55 |
| | (2.98-2.83)[a] | (3.37-3.2) | (1.63-1.55) |
| No. reflections | 22,497 | 17,105 | 145,853 |
| Unique reflections | 6,845 | 6,186 | 42,168 |
| R-merge[b] (%)[a] | 9.3 (49.8) | 24.6 (52.7) | 6.8 (49.8) |
| I/σ(I)[a] | 8.6 (2.5) | 3.4 (2.0) | 9.8 (2.7) |
| Completeness (%)[a] | 95.8 (97.7) | 99.2 (99.5) | 97.6 (97.5) |
| Multiplicity[a] | 3.3 (3.4) | 2.8 (2.8) | 3.5 (3.5) |
| | | | |
| **Refinement statistics:** | | | |
| R-factor[c]/R-free (%) | 25.5/29.7 | 20.9/24.0 | 15.6/20.4 |
| Protein residues | 258 | 306 | 307 |
| | (A: 6-47, 68-157) | (A:3-157) | (A: 5-158) |
| | (B: 7-45, 70-156) | (B: 3-56, 61-157) | (B: 3-155) |
| Heme groups | 2 | 2 | 3 |
| Water molecules | 4 | 30 | 171 |
| Glycerol molecules | - | - | 2 |
| Imidazole molecules | - | - | 1 |
| r.m.s.deviation from ideality: | | | |
| Bond lengths (Å) | 0.011 | 0.010 | 0.017 |
| Bond angles (°) | 1.97 | 1.45 | 1.81 |
| Ramachandran plot (%): | | | |
| Most favored | 88.1 | 92.3 | 98.7 |



Antioxidants and Redox Signaling
Structural and functional characterization of the globin-coupled sensors of *Azotobacter vinelandii* and *Bordetella pertussis* (DOI: 10.1089/ars.2018.7690)
This paper has been peer-reviewed and accepted for publication, but has yet to undergo copyediting and proof correction. The final published version may differ from this proof.

| | | | |
|---|---|---|---|
| Additionally allowed | 11.9 | 7.7 | 1.3 |
| Disallowed regions | 0.0 | 0.0 | 0.0 |

[a] Highest resolution shell parameters are in parentheses

[b] R-merge = $\Sigma_h\Sigma_i \mid I_{hi} - \langle I_h \rangle \mid / \Sigma_h\Sigma_i I_{hi}$

[c] R-factor = $\Sigma_h \mid\mid F_{obs}\mid - \mid F_{calc}\mid\mid / \Sigma_h \mid F_{obs}\mid$, with $F_{obs}$ being the observed and $F_{calc}$ the calculated structure factor amplitudes



Antioxidants and Redox Signaling
Structural and functional characterization of the globin-coupled sensors of *Azotobacter vinelandii* and *Bordetella pertussis* (DOI: 10.1089/ars.2018.7690)
This paper has been peer-reviewed and accepted for publication, but has yet to undergo copyediting and proof correction. The final published version may differ from this proof.

## Figure legends

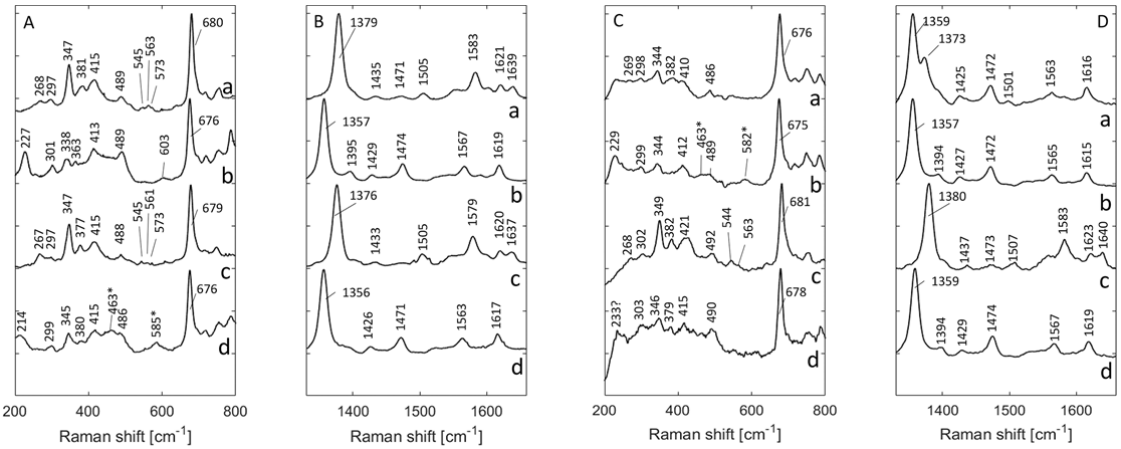


**Figure 1. Resonance Raman spectra of *Av*GReg.**

RR spectra of *Av*GReg (a,b) and *Av*GReg-Gb (c,d) in the low-frequency region (**A**) and high-frequency region (**B**) and RR spectra of *Bpe*GReg (a,b) and *Bpe*GReg-Gb (c,d) in the low-frequency region (**C**) and high-frequency region (**D**). Traces (a,c) show the RR spectra of the proteins as purified (oxygenated Fe(II) state), traces (b,d) show the RR spectra of the dithionite-reduced proteins (ferrous state). Wavenumbers marked with asterisk indicate reminiscent contributions of dithionite as described in (8).



Antioxidants and Redox Signaling
Structural and functional characterization of the globin-coupled sensors of *Azotobacter vinelandii* and *Bordetella pertussis* (DOI: 10.1089/ars.2018.7690)
This paper has been peer-reviewed and accepted for publication, but has yet to undergo copyediting and proof correction. The final published version may differ from this proof.

Antioxidants and Redox Signaling
Structural and functional characterization of the globin-coupled sensors of *Azotobacter vinelandii* and *Bordetella pertussis* (DOI: 10.1089/ars.2018.7690)
This paper has been peer-reviewed and accepted for publication, but has yet to undergo copyediting and proof correction. The final published version may differ from this proof.

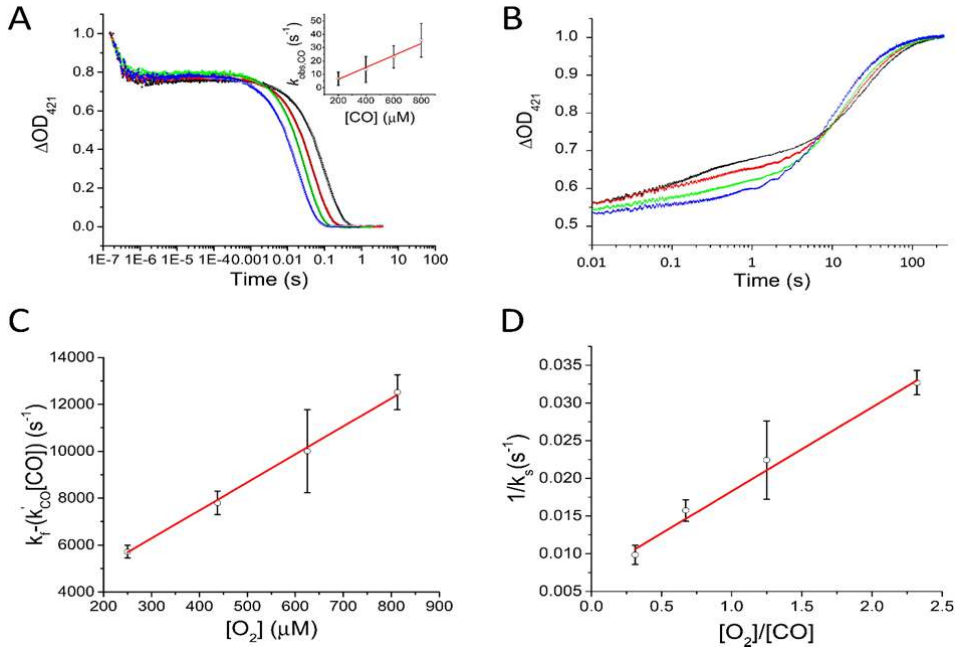


**Figure 2. Ligand binding kinetics curves for *Av*GReg.**

(**A**) Experimental curves of the CO-rebinding to *Av*GReg (black: 200 μM CO, red: 400 μM CO, green: 600 μM CO, blue: 800 μM CO). The dependence of the pseudo-first order constants of CO binding ($k_{obsCO}$) to *Av*GReg on the relative ligand concentration is reported in the inset. (**B**) Stopped-flow $O_2$/CO replacement experimental curves of *Av*GReg (black: 50% CO - 50% $O_2$, red: 60% CO - 40% $O_2$, green: 70% CO - 30% $O_2$, blue: 80% CO - 20% $O_2$). The *fast* and the *slow* replacement phases are detectable for all the gas ratios used. (**C**) Dependence of the apparent $k_f$ constants of $O_2$ binding to *Av*GReg on the relative ligand concentration. (**D**) Dependence of the apparent $k_s$ constants of CO binding to *Av*GReg on the relative ligand concentration. Experimental values are reported with open circles, while the theoretical ligand-binding mechanism is represented with a straight line.

Antioxidants and Redox Signaling
Structural and functional characterization of the globin-coupled sensors of *Azotobacter vinelandii* and *Bordetella pertussis* (DOI: 10.1089/ars.2018.7690)
This paper has been peer-reviewed and accepted for publication, but has yet to undergo copyediting and proof correction. The final published version may differ from this proof.

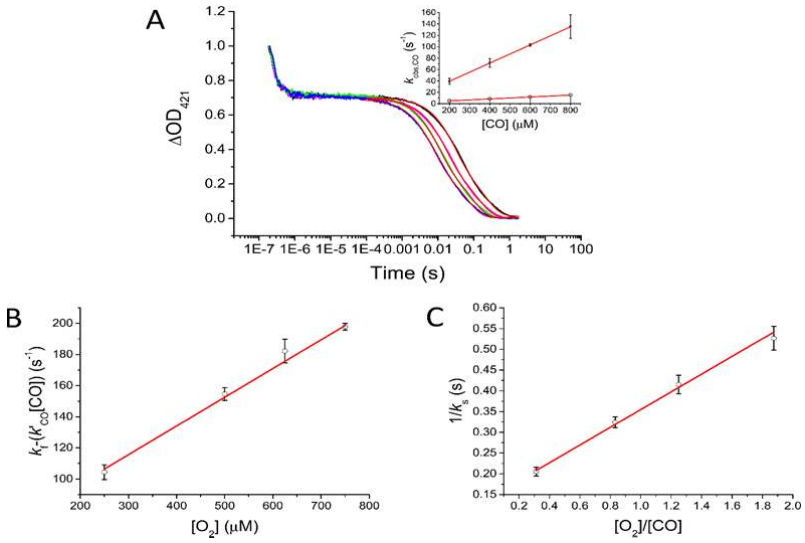


**Figure 3. Ligand binding kinetics curves for *Bpe*GReg.**

(**A**) Experimental CO-rebinding decays to *Bpe*GReg (black: 200 µM CO, magenta: 400 µM CO, green: 600 µM CO, blue: 800 µM CO) with the corresponding fitting curves (in red color). The dependence of the second order constants of CO binding ($k_{obsCO}$) to *Bpe*GReg on the relative ligand concentration is reported in the inset. Experimentally obtained values are indicated with closed (fast rebinding) and open (slow rebinding) circles, the theoretical fitting lines are reported in red. (**B**) Dependence of the apparent $k_f$ constants of $O_2$ binding to *Bpe*GReg on the relative ligand concentration. (**C**) Dependence of the apparent $k_s$ constants of CO binding to *Bpe*GReg on the relative ligands concentration ratio. Experimental values are reported with open circles, while the theoretical ligand-binding mechanism is represented with red lines.

Antioxidants and Redox Signaling
Structural and functional characterization of the globin-coupled sensors of *Azotobacter vinelandii* and *Bordetella pertussis* (DOI: 10.1089/ars.2018.7690)
This paper has been peer-reviewed and accepted for publication, but has yet to undergo copyediting and proof correction. The final published version may differ from this proof.

**A**

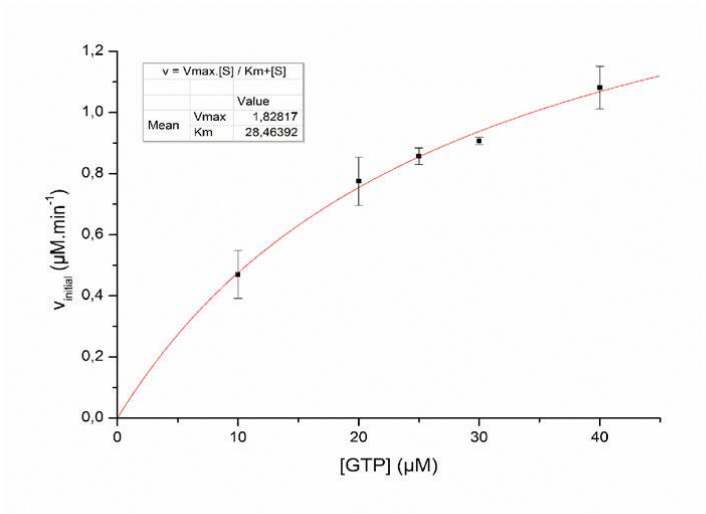


**B**

| | Measurement 1 | Measurement 2 | Measurement 3 | Average | STDEV |
|---|---|---|---|---|---|
| $V_{max}$ | 1.86 µM.min$^{-1}$ | 1.90 µM.min$^{-1}$ | 1.70 µM.min$^{-1}$ | 1.82 µM.min$^{-1}$ | 0.08 µM.min$^{-1}$ |
| $K_m$ | 23.6 µM | 30.9 µM | 26.5 µM | 27.0 µM | 3.0 µM |
| $K_{cat}$ / $K_m$ | 0.787 µM$^{-1}$.min$^{-1}$<br>1.31 x10$^4$ M$^{-1}$.s$^{-1}$ | 0.614 µM$^{-1}$.min$^{-1}$<br>1.02 x10$^4$ M$^{-1}$.s$^{-1}$ | 0.640 µM$^{-1}$.min$^{-1}$<br>1.06 x10$^4$ M$^{-1}$.s$^{-1}$ | 0.680 µM$^{-1}$.min$^{-1}$<br>1.13 x10$^4$ M$^{-1}$.s$^{-1}$ | 0.076 µM$^{-1}$.min$^{-1}$<br>0.13 x10$^4$ M$^{-1}$.s$^{-1}$ |

**Figure 4. Enzymatic characteristics of the DGC activity of *Av*GReg.**

(**A**) Reaction rate. (**B**) Summary of 3 independent measurements.

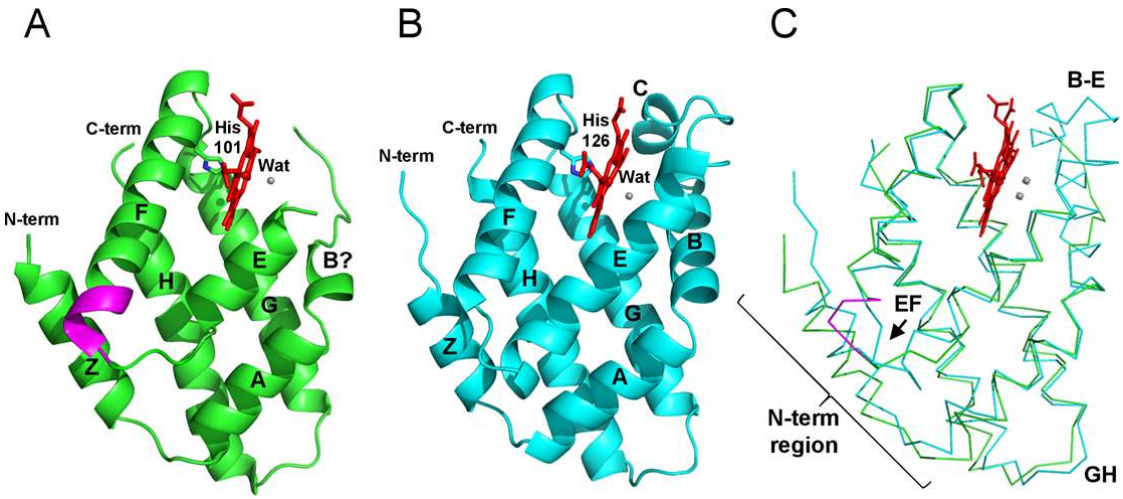


**Figure 5. Tertiary structures.**

Ribbon representation of the tertiary structure of (**A**) *Av*GReg-Gb (green) and (**B**) *Bpe*GReg-Gb* (cyan). Helices are labelled accordingly with the globin fold nomenclature. The extra-turn of the F helix of *Av*GReg-Gb is shown in magenta. Proximal His residues and $Fe^{3+}$-ligated water molecules are indicated. (**C**) Cα-trace overlay of the *Av*GReg-Gb A (green) and *Bpe*GReg-Gb* (cyan). Regions displaying the main structural differences are highlighted.



Antioxidants and Redox Signaling
Structural and functional characterization of the globin-coupled sensors of *Azotobacter vinelandii* and *Bordetella pertussis* (DOI: 10.1089/ars.2018.7690)

Antioxidants and Redox Signaling
Structural and functional characterization of the globin-coupled sensors of *Azotobacter vinelandii* and *Bordetella pertussis* (DOI: 10.1089/ars.2018.7690)
This paper has been peer-reviewed and accepted for publication, but has yet to undergo copyediting and proof correction. The final published version may differ from this proof.

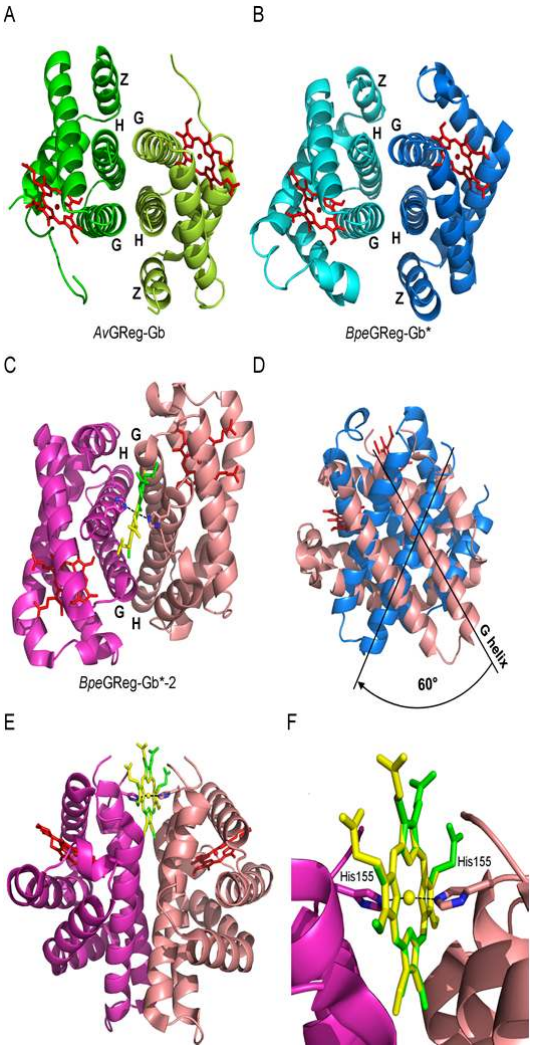


**Figure 6. Quaternary structures.**

Top view of (**A**) the *Av*GReg-Gb dimer, and (**B**) the *Bpe*GReg-Gb* dimer, with the two subunits interacting mainly through the G- and H-helices (helical bundle), shown as ribbon models. The heme groups are shown in red. (**C**) Dimeric arrangement of *Bpe*GReg-Gb*-2. The dimeric interface involves the G- and H-helices as in the *Bpe*GReg-Gb* dimer, but the subunits are oriented differently. (**D**) Relative orientation of the B subunits of *Bpe*GReg-Gb* (blue) and *Bpe*GReg-Gb*-2 (pink), after superimposing the two A chains (omitted in the picture for clarity). The rotation of 60° is highlighted, taking the position of the G helices as reference. (**E**, **F**) The heme group at the top of the *Bpe*GReg-Gb*-2 dimer is modelled in two conformations (green and yellow) with 0.5 occupancy each, with the Fe-atom hexacoordinated to the His155 side chain of the two subunits of the dimer.

Antioxidants and Redox Signaling

Structural and functional characterization of the globin-coupled sensors of *Azotobacter vinelandii* and *Bordetella pertussis* (DOI: 10.1089/ars.2018.7690)

This paper has been peer-reviewed and accepted for publication, but has yet to undergo copyediting and proof correction. The final published version may differ from this proof.

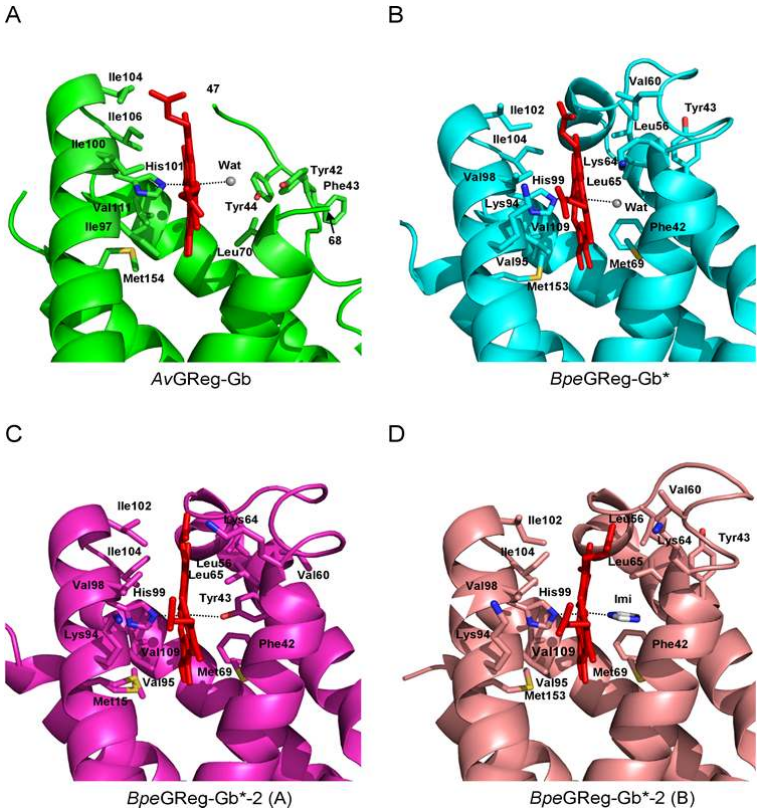


**Figure 7. Proximal and distal sites.**

The figure shows the main residues building the heme proximal and distal sites for (**A**) *Av*GReg-Gb (A chain), (**B**) *Bpe*GReg-Gb* (A chain), (**C,D)** *Bpe*GReg-Gb*-2 (A and B chains). The *Av*GReg-Gb and *Bpe*GReg-Gb* distal sites host a water molecule (gray) coordinated to the heme-$Fe^{3+}$. In *Bpe*GReg-Gb*-2 a coordination with Tyr43 is present in the A chain, while an imidazole molecule is bound in the B chain.

## Supplementary legends

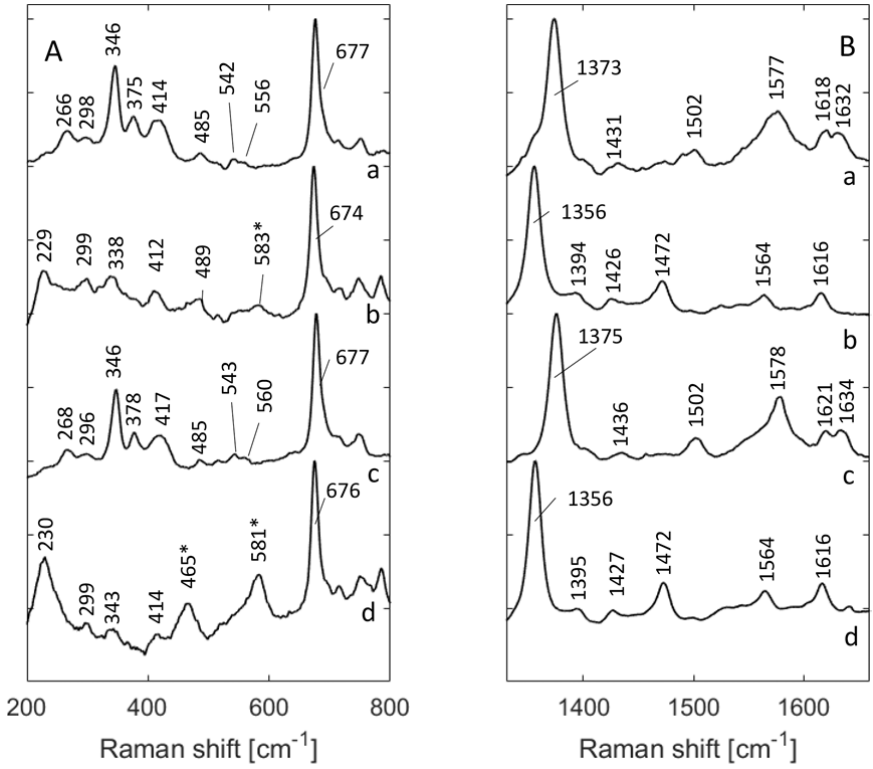


**Figure S1. Resonance Raman spectra of *Bpe*GReg* and *Bpe*GReg-Gb*.**

RR spectra of *Bpe*GReg* (a,b) and *Bpe*GReg-Gb* (c,d) in the low-frequency region (**A**) and high-frequency region (**B**). Traces (a,c) show the RR spectra of the proteins as purified (oxygenated Fe(II) state), traces (b,d) show the RR spectra of the dithionite-reduced proteins (ferrous state). Wavenumbers marked with asterisk indicate reminiscent contributions of dithionite as described in (8). These signals hamper the analysis of the low-frequency region of the RR spectrum of *Bpe*GReg-Gb*.



Antioxidants and Redox Signaling
Structural and functional characterization of the globin-coupled sensors of *Azotobacter vinelandii* and *Bordetella pertussis* (DOI: 10.1089/ars.2018.7690)
This paper has been peer-reviewed and accepted for publication, but has yet to undergo copyediting and proof correction. The final published version may differ from this proof.

Antioxidants and Redox Signaling
Structural and functional characterization of the globin-coupled sensors of *Azotobacter vinelandii* and *Bordetella pertussis* (DOI: 10.1089/ars.2018.7690)
This paper has been peer-reviewed and accepted for publication, but has yet to undergo copyediting and proof correction. The final published version may differ from this proof.

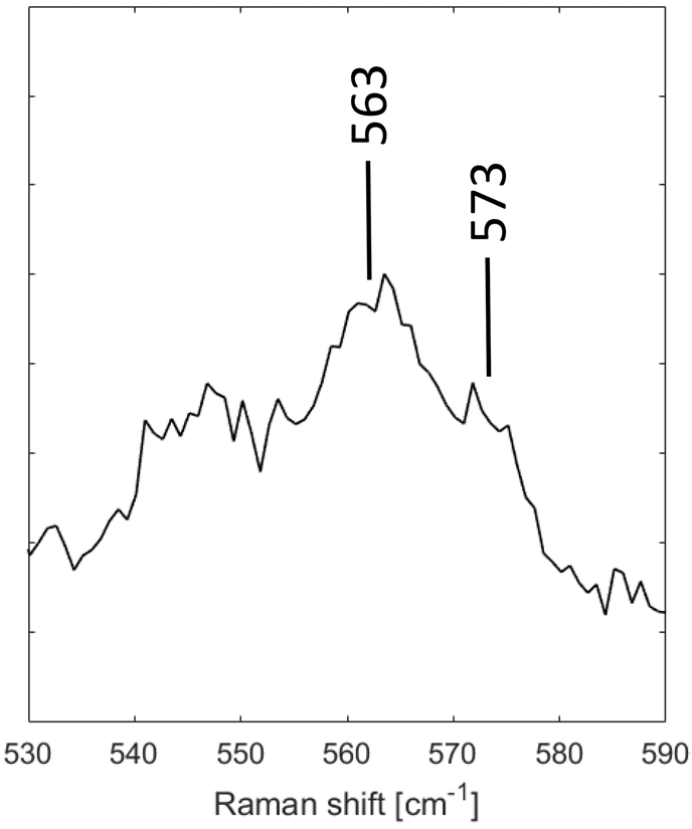


**Figure S2. Detailed Resonance Raman spectrum of $O_2$-*Av*GReg.**

The figure zooms in on the region in which the Fe-$O_2$ modes are visible.

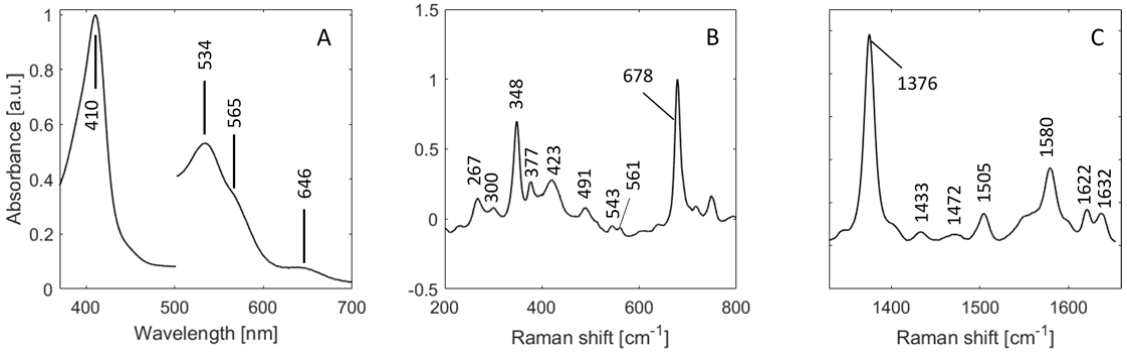


**Figure S3. UV/Vis absorption (A) and Resonance Raman (B,C) spectra of ferric *Av*GReg.**

*Av*GReg was oxidized by addition of potassium ferricyanide. (**A**) The Soret and Q-bands confirm the oxidation to a ferric low-spin form. However, the presence of a peak at 646 nm indicates that also partial degradation has taken place (formation of hemochrome derivatives, like biliverdin). (**B,C**) The RR spectra are similar to those observed previously for the *in-vivo* refolded $^{\dagger}$*Av*GReg (64). RR peaks confirm the assignment from (prominent peaks at $\nu_3$=1505 $cm^{-1}$ confirms the low-spin (hexa-coordination of the heme)). Additionally, the observation of small peaks in the area of 545-565 $cm^{-1}$ indicate that some of the proteins are still in the oxygenated ferrous form. Interestingly, the 573 $cm^{-1}$ peak has disappeared indicating that this open configuration of the heme group oxidizes the easiest.



Antioxidants and Redox Signaling
Structural and functional characterization of the globin-coupled sensors of *Azotobacter vinelandii* and *Bordetella pertussis* (DOI: 10.1089/ars.2018.7690)
This paper has been peer-reviewed and accepted for publication, but has yet to undergo copyediting and proof correction. The final published version may differ from this proof.

Antioxidants and Redox Signaling
Structural and functional characterization of the globin-coupled sensors of *Azotobacter vinelandii* and *Bordetella pertussis* (DOI: 10.1089/ars.2018.7690)
This paper has been peer-reviewed and accepted for publication, but has yet to undergo copyediting and proof correction. The final published version may differ from this proof.

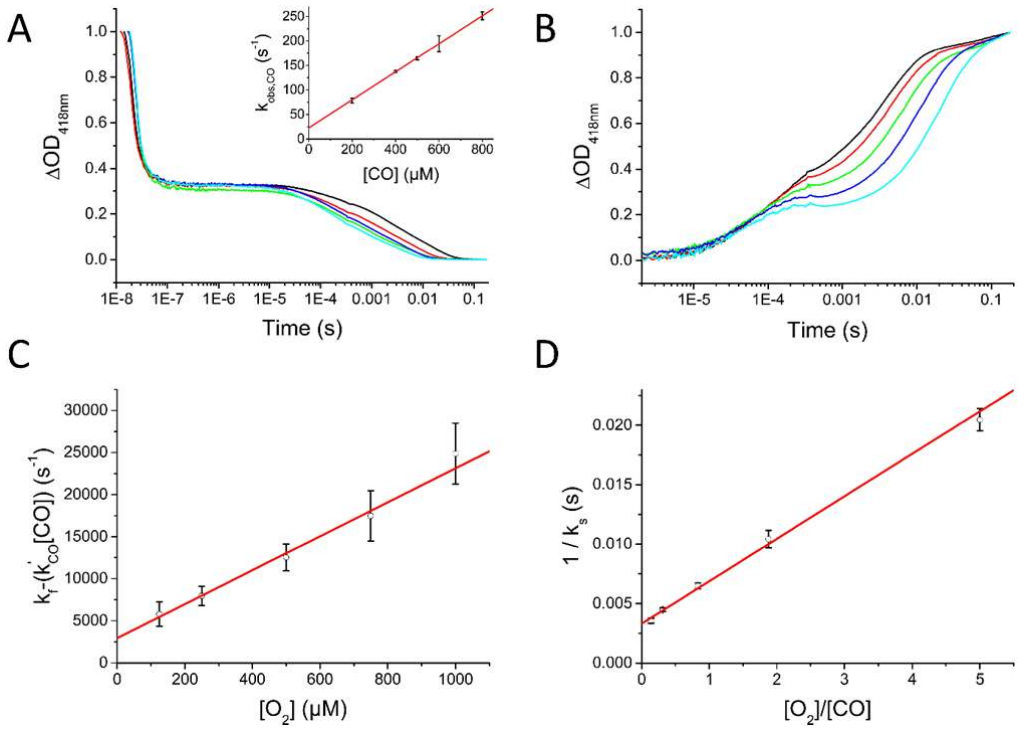


**Figure S4. Ligand binding kinetics curves for *Av*GRegYB10F.**

(**A**) Experimental curves of the CO-rebinding to *Av*GRegYB10F (black: 200 µM CO, red: 400 µM CO, green: 500 µM CO, blue: 600 µM CO, cyan: 800 µM CO). The dependence of the pseudo-first order constants of CO binding ($k_{obsCO}$) to *Av*GReg YB10F on the relative ligand concentration is reported in the inset. (**B**) Stopped-flow $O_2$/CO replacement experimental curves of *Av*GRegYB10F (black: 90% CO - 10% $O_2$, red: 80% CO - 20% $O_2$, green: 60% CO - 40% $O_2$, blue: 40% CO - 60% $O_2$, cyan: 20% CO - 80% $O_2$). The *fast* and the *slow* replacement phases are detectable for all the gas ratios used. (**C**) Dependence of the apparent $k_f$ constants of $O_2$ binding to *Av*GRegYB10F on the relative ligand concentration. (**D**) Dependence of the apparent $k_s$ constants of CO binding to *Av*GRegYB10F on the relative ligand concentration. Experimental values are reported with open circles, while the theoretical ligand-binding mechanism is represented with a straight line.